

technology) and developed with horseradish peroxidase-coupled secondary antibodies, followed by enhancement with a chemiluminescence (ECL) detection system (GE Healthcare).

Generation of Adenoviruses—Adenoviruses carrying GFP or Cry1 were constructed using the ViraPower Adenoviral Expression System (Invitrogen). Briefly, cDNA was inserted into a TOPO pENTR vector and was recombined to the adenovirus expression plasmid pAd/CMV/V5-DEST. The pAd/CMV/V5-DEST plasmid with the cDNA of interest was digested with the PaeI endonuclease and transfected with HEK293A cells. The medium supernatant containing the adenovirus was collected and titrated according to the manufacturer's instructions. UMR-106 cells were infected with the adenovirus at a multiplicity of infection of 500 with 4 $\mu\text{g/ml}$ poly-L-lysine (Sigma).

Constructs and Luciferase Reporter Assay—The Cry1 expression construct with a V5 tag was created by subcloning the corresponding PCR products into the pENTR vector using the pENTR Directional TOPO cloning kit (Invitrogen) and transferring to the pcDNA3.2/V5 vectors using the LR recombination reaction system (Invitrogen). Luciferase vectors containing 2000 bp of the mouse *Fgf23* gene promoter (−1872 to +128) (2000bp-Luc) was prepared by subcloning the corresponding PCR products into pGL4.20[luc2/Puro] (Promega, Madison, WI) vectors according to the previous report (13). Luciferase constructs containing 766 bp (−638 to +128) of the *Fgf23* gene promoter were created by the digestion of 2000bp-Luc with BglII (located at the 5' region in the multiple cloning site of the pGL4.20 vector relative to the insert and −638 to −633) followed by the ligation of fragments containing luciferase with T4 DNA ligase. Luciferase constructs containing 143 bp (−15 to +128) of the *Fgf23* gene promoter were designed by digesting pT7 vectors harboring 2000 bp of the *Fgf23* gene promoter with SmaI (located at −18 to −13 and the 3' region in the pT7 vector relative to the insert) followed by the ligation of fragments containing the promoter region of interest with pGL4.20[luc2/Puro] vectors digested with EcoRV using T4 DNA ligase.

Mutagenesis—Two candidate motifs were detected as possible cAMP responsive elements (CREs) in the promoter region of the *Fgf23* gene by *in silico* analysis, and these motifs were designated as CRE1 and CRE2, respectively. To determine whether these motifs were functional, site-directed mutagenesis was performed using QuikChange II XL (Agilent Technologies, Santa Clara, CA) according to the manufacturer's protocol. The CRE1 located at −620 to −613 and CRE2 located at −46 to −39 were mutated from TGACCTCA to TGAAATCA and TGATGTCA to TGAAATCA, respectively.

Luciferase Assay—UMR-106 cells were seeded in a 24-well plate at a density of 5×10^4 cells/well, and transient transfection was carried out using FuGENE HD (Promega) following the manufacturer's protocol. The total amount of DNA added to each well was equalized using an empty vector. The luciferase assay was performed in triplicate according to the protocol of the dual-luciferase reporter assay system (Promega). Briefly, 24 h after transfection cells were treated with isoproterenol (10 or 100 μM) and/or IBMX (0.5 mM) in DMEM containing 1% FCS overnight, followed by the determination of luciferase activity using specific substrates in a luminometer. Transfec-

tion efficiency was normalized by co-transfection with the TK-*Renilla* luciferase construct (Promega). While Cry1-overexpressing UMR-106 cells were used for the luciferase assay, UMR-106 cells were infected with an adenovirus containing GFP or Cry1-V5. Twenty-four h after the infection cells were trypsinized and plated in a 24-well plate as described above.

Animal Studies—Isoproterenol or PTH(1–34) was dissolved in saline and administered intraperitoneally at a dose of 6 $\mu\text{g/g}$ (32) or 100 $\mu\text{g/kg}$, respectively. A saline injection was used as a control treatment. Whereas propranolol (PRO) was used for the *in vivo* study, PRO was dissolved in the drinking water at a concentration of 0.5 g/liter (33), and the drinking water was changed three times a week.

Measurement of Serum and Urine Parameters—The measurement of serum phosphate was carried out using P-test Wako (Wako Pure Chemical Industries Ltd., Osaka, Japan). Total (C-Term) and intact (full-length) FGF23 concentrations were determined by ELISA from Immotopics, Inc., San Clemente, CA and Kainos Laboratory, Tokyo, Japan, respectively, following the manufacturers' instructions. Urine samples were collected in the presence of 5 μl of 5 N HCl, and the volume of urine was measured. Urine epinephrine was determined using ELISA (IBL, Hamburg, Germany). Urine phosphate and creatinine were measured using P-test Wako and Creatinine Test Kit (Wako Pure Chemical Industries Ltd.), respectively.

Statistical Analysis—All data are expressed as the mean \pm S.E. Results were examined for significant differences using Student's *t* test or analysis of variance followed by the Bonferroni multiple comparison *post hoc* test. Significance was set at $p < 0.05$.

RESULTS

Skeletal *Fgf23* Exhibited a Circadian Expression Profile—To investigate the mechanisms whereby phosphate metabolism is regulated by the circadian clock network, we first examined the circadian expression profile of *Fgf23* in the femur of wild-type mice fed standard chow *ad libitum* (AL). As reported previously (34), components of the clock network including *Rev-erba* (nuclear receptor subfamily 1, group D, member 1; Nr1d1), *Dbp* (D site of albumin-binding protein), and *Cry1* exhibited rhythmic expression patterns in the femur (Fig. 1, A–C, and supplemental Fig. S1). The *Fgf23* expression profile showed higher expression levels during the dark phase (DP) compared with the light phase (LP) with the highest at ZT16 (Fig. 1D and supplemental Fig. S1). Because it is well known that food consumption reaches highest at the beginning of DP in mice fed AL, we speculated that skeletal *Fgf23* expression was regulated by the food consumption in a manner involving the circadian clock system. To test this speculation, mice were fed during the LP from ZT2 to ZT8 (LP-restricted feeding; LP-RF) for 10 days. Because it is unclear whether skeletal tissue is entrained by nutrient availability despite the fact that food intake is a strong zeitgeber in peripheral tissues such as liver, we examined the circadian expression profiles of genes involved in daily oscillations in the femur. As shown in Fig. 2, A–C, and supplemental Fig. S2, the peak expressions of *Rev-erba*, *Dbp*, and *Cry1* shifted by 12 h in mice under LP-RF conditions compared with AL conditions, suggesting that skeletal tissue is also

FGF23 and Circadian Clock Network

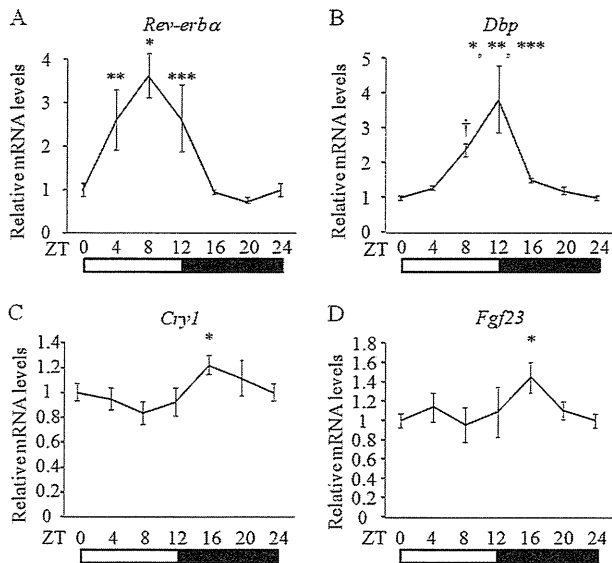


FIGURE 1. *Fgf23* showed a rhythmic expression pattern in the femur of mice fed *ad libitum*. WT mice were maintained under a light-dark regimen (12-h:12-h cycle) and fed *ad libitum*. Samples were collected every 4 h from ZT0. **A**, expression of *Rev-erbα* ($n = 3-4$, *, $p < 0.01$ versus ZT0 and ZT20; **, $p < 0.05$ versus ZT20; ***, $p < 0.05$ versus ZT0, ZT16 and ZT20). **B**, expression of *Dbp* ($n = 3$, *, $p < 0.001$ versus ZT0, ZT4, and ZT20; **, $p < 0.01$ versus ZT16; ***, $p < 0.05$ versus ZT8; †, $p < 0.05$ versus ZT0). **C**, expression of *Cry1* ($n = 5-7$, *, $p < 0.05$ versus ZT8). **D**, expression of *Fgf23* ($n = 5-7$, *, $p < 0.05$ versus ZT8). All expression was in the femur and was analyzed using real-time RT-PCR. The white bar and black bar represent the light phase and dark phase, respectively. Values are expressed as the mean \pm S.E. (error bars).

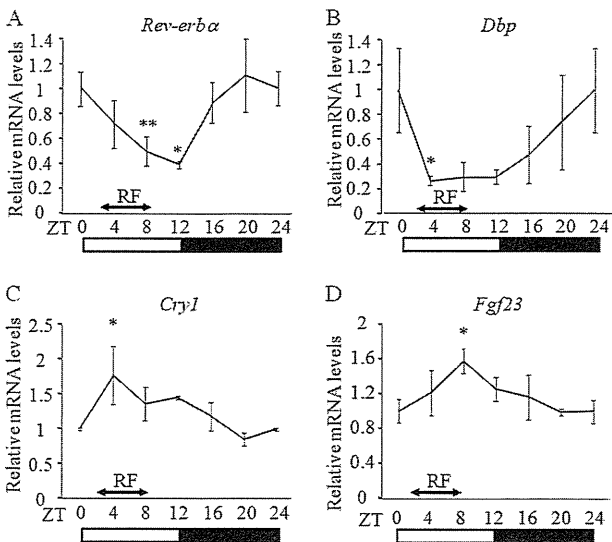


FIGURE 2. Light phase restricted feeding altered the expression profile of *Fgf23* in the femur. WT mice were maintained under a light-dark regimen (12-h:12-h cycle) and fed for 6 h from ZT2 to ZT8 for 10 days. Samples were collected every 4 h from ZT0. **A**, expression of *Rev-erbα* ($n = 3$, *, $p < 0.05$ versus ZT0 and ZT20; **, $p < 0.05$ versus ZT20). **B**, expression of *Dbp* ($n = 3$, *, $p < 0.05$ versus ZT0). **C**, expression of *Cry1* ($n = 3-4$, *, $p < 0.05$ versus ZT0 and ZT20). **D**, expression of *Fgf23* ($n = 3$, *, $p < 0.05$ versus ZT0). All expression was in the femur and was determined by real-time RT-PCR. The white bar and black bar represent the light phase and dark phase, respectively. Values are expressed as the mean \pm S.E. (error bars).

entrained by nutrient availability. Based on this observation, we next analyzed the expression profile of *Fgf23* in the femur and found that *Fgf23* showed a rhythmic expression pattern with a peak expression at ZT8 (Fig. 2D and supplemental Fig. S2). Taken together, these findings indicate that *Fgf23* expression

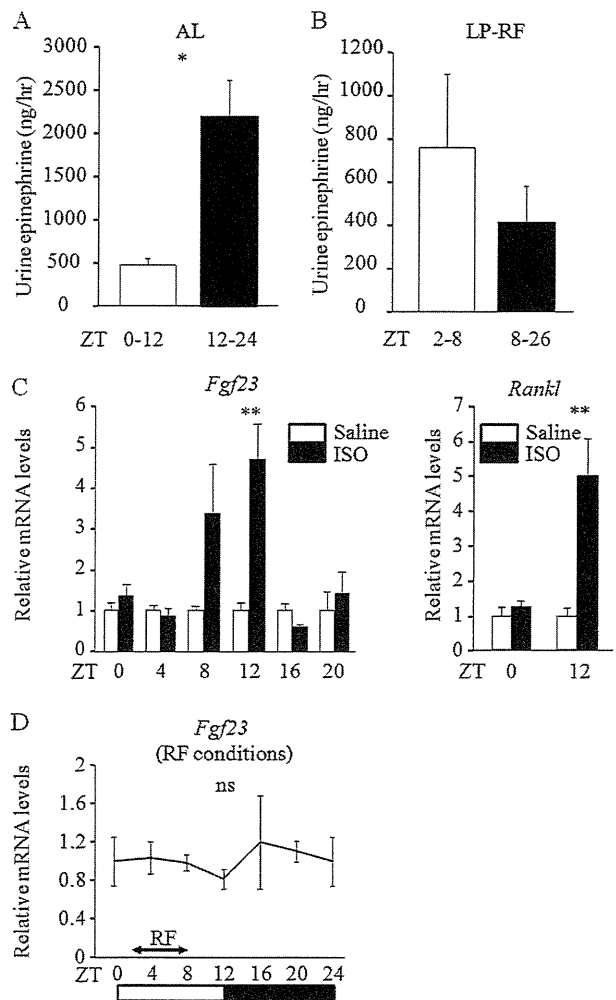


FIGURE 3. Sympathetic activation induced skeletal *Fgf23* expression *in vivo*. **A**, urine was collected from WT mice under *ad libitum* (AL) conditions either during the light phase (LP: ZT0-12) or the dark phase (ZT12-24). The volume of urine and urine epinephrine levels were measured, and the amount of urine epinephrine/h was determined ($n = 9$). **B**, urine was collected from WT mice under LP-RF conditions either during ZT2-8 or ZT8-26. The volume of urine and urine epinephrine levels were measured, and the amount of urine epinephrine/h was determined ($n = 7$). **C**, ISO was administered intraperitoneally to WT mice under AL conditions at different time points of the day as indicated, and 4 h after the injection the expression of *Fgf23* and *Rankl* in the femur was determined by real-time RT-PCR ($n = 3-4$). **D**, WT mice were maintained under LP-RF conditions for 10 days, and 0.5 g/liter propranolol was added to the drinking water from day 7 to day 10. Femurs were collected at indicated time points, and *Fgf23* expression was measured by real-time RT-PCR ($n = 3$). The white bar and black bar represent the light phase and dark phase, respectively. ns, not significantly different. Values are expressed as the mean \pm S.E. (error bars). *, $p < 0.001$; **, $p < 0.05$.

possesses a circadian expression profile that is at least in part determined by the time of nutrient availability.

Sympathetic Activation Enhanced *Fgf23* Expression in the Femur—It is well known that food intake is tightly coupled to an increase in the metabolic rate to adjust for the increase in nutrient influx, which in part involves an elevation in sympathetic activity (25–28). Indeed, urine levels of epinephrine, a marker for sympathetic activity, in mice fed AL were significantly enhanced in DP compared with LP (Fig. 3A). Interestingly, LP-RF caused a phase shift in sympathetic activity with greater levels during LP-RF, but the difference did not reach statistical significance (Fig. 3B). Based on these findings, we speculated

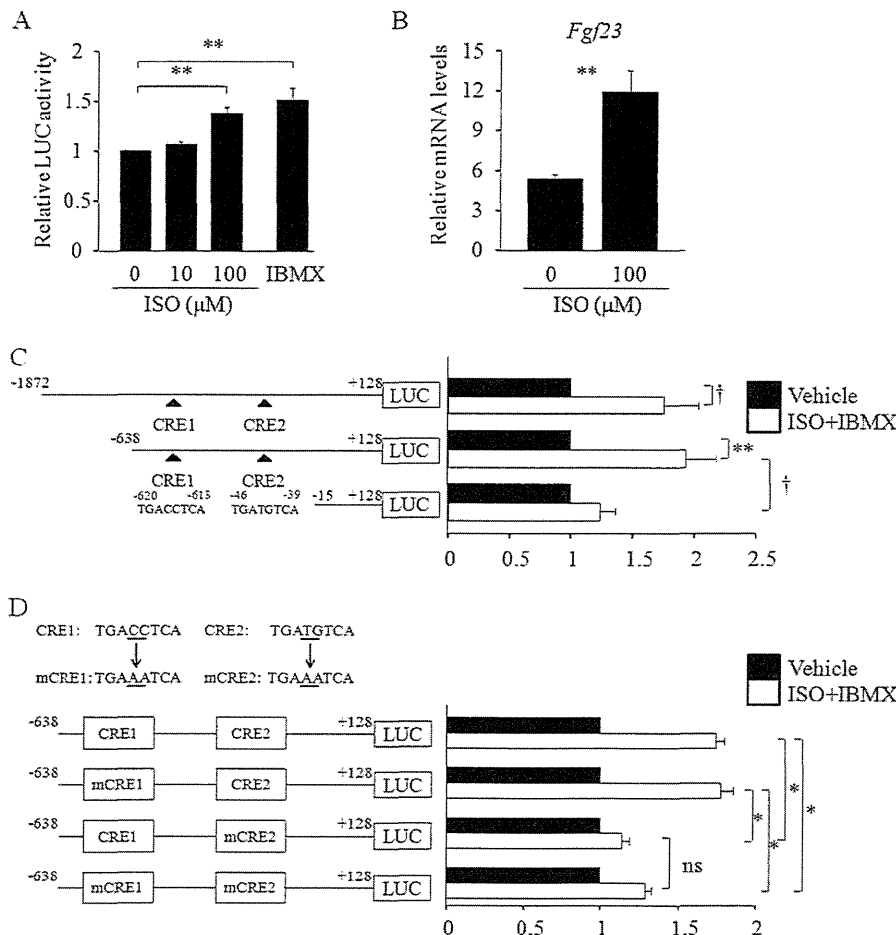


FIGURE 4. ISO trans-activated *Fgf23* transcription in UMR-106 cells. *A*, UMR-106 cells were seeded in 24-well plates and transfected with 2000bp-Luc (200 ng) and phRL-TK (10 ng). Twenty-four h after transfection, cells were treated with ISO at a dose of 10 or 100 μM overnight, and luciferase activity was measured. 0.5 mM IBMX was used as a positive control for the activation of cAMP signaling ($n = 3$). *B*, UMR-106 cells were treated with 100 μM ISO overnight, and expression of *Fgf23* was determined by real-time RT-PCR ($n = 4$). *C*, UMR-106 cells were seeded in 24-well plates and transfected with 2000bp-Luc (200 ng), 766bp-Luc (200 ng), or 143bp-Luc (200 ng) and phRL-TK (10 ng). Twenty-four h after transfection, cells were treated with ISO (100 μM) and IBMX (0.5 mM) overnight, and luciferase activity was measured ($n = 5$). *D*, UMR-106 cells were seeded in 24-well plates and transfected with 766bp-Luc (200 ng) or 766bp-Luc containing mutations in CRE1 and/or CRE2 (200 ng), and phRL-TK (10 ng). Twenty-four h after transfection, cells were treated with ISO (100 μM) and IBMX (0.5 mM) overnight, and luciferase activity was measured ($n = 4$). Values are expressed as the mean ± S.E. (error bars). *ns*, not significantly different. *, $p < 0.001$; **, $p < 0.01$; †, $p < 0.05$.

that *Fgf23* expression may at least in part be regulated by sympathetic activation in a circadian manner. To test this idea, we intraperitoneally administered the β-adrenergic receptor agonist, isoproterenol (ISO), to mice at different time points of the day and analyzed the expression of *Fgf23* in the femur 4 h after the injection. The administration of ISO caused an increase in skeletal *Fgf23* expression when injected at ZT8 ($p = 0.12$) and ZT12 ($p < 0.05$), whereas ISO treatment had no effect on *Fgf23* expression when administered at the other time points (Fig. 3C). To determine whether the effect of ISO was specific to *Fgf23* induction, we also analyzed the expression of *Rankl*, one of the target genes of ISO (35), and found that the induction of *Rankl* showed a pattern similar to that of *Fgf23* induction (Fig. 3C). To further understand the involvement of sympathetic activity in the circadian *Fgf23* profile, mice were maintained under LP-RF in the presence of the β-blocker, PRO, to analyze the effect of sympathetic activity on the peak expression of *Fgf23* noted at ZT8. Interestingly, *Fgf23* expression did not exhibit any circadian profile when PRO was concomitantly administered, indicating the involvement of sympathetic activ-

ity in the circadian profile of *Fgf23* expression in the femur (compare Fig. 3D with Fig. 2D, and see supplemental Fig. S2).

ISO Trans-activated the *Fgf23* Gene Promoter and Induced *Fgf23* Expression in UMR-106 Cells—Because *in vivo* administration of ISO enhanced the expression of *Fgf23* in the femur, we investigated whether ISO signaling trans-activated *Fgf23* gene promoter using osteoblastic UMR-106 cells in which endogenous *Fgf23* was expressed. For this purpose, we generated a luciferase construct containing a 2000-bp promoter region of the mouse *Fgf23* gene. The treatment with ISO showed a significant increase in luciferase activity in a dose-dependent manner (Fig. 4A). In line with this, the ISO treatment enhanced the expression of *Fgf23* in these cells (Fig. 4B). These results suggest that ISO induces *Fgf23* expression at least in part by activating the transcription of the *Fgf23* gene. Because *in silico* analysis pointed out the existence of two motifs whose sequences were very similar to CRE, we next tested whether these motifs, designated as CRE1 and CRE2, respectively, were involved in ISO-induced *Fgf23* trans-activation. For this purpose, we generated luciferase vectors containing the truncated

FGF23 and Circadian Clock Network

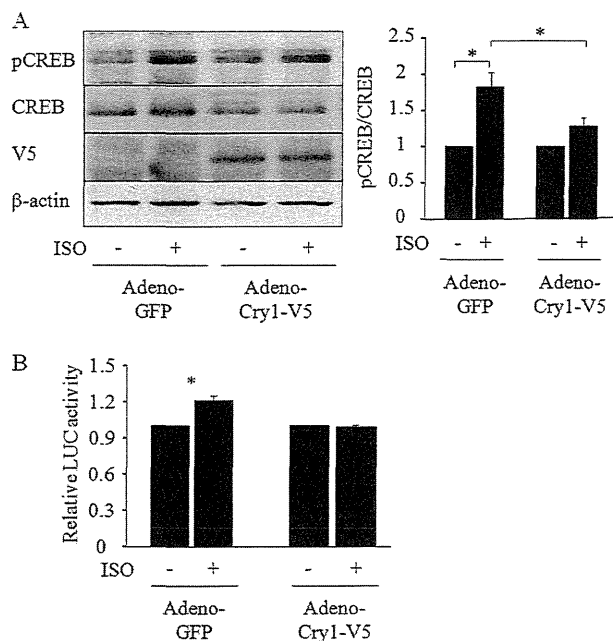


FIGURE 5. Cry1 suppressed ISO-induced phosphorylation of CREB in UMR-106 cells. *A*, UMR-106 cells were infected with an adenovirus containing GFP or Cry1-V5 and treated with 100 μ M ISO for 5 min. The expression of pCREB, CREB, V5, and β -actin was determined by Western blotting, and expression of pCREB was quantified by normalizing to the levels of CREB by densitometric analysis ($n = 5$). *B*, UMR-106 cells infected with an adenovirus containing either GFP or Cry1 were seeded in 24-well plates and transfected with 2000bp-Luc (200 ng) and phRL-TK (10 ng). Twenty-four h after transfection cells were treated with 100 μ M ISO overnight, and luciferase activity was measured ($n = 3$). The figures shown are the representative from at least three independent experiments. Values are expressed as the mean \pm S.E. (error bars). *, $p < 0.05$.

forms of the *Fgf23* gene promoter and found that the luciferase vectors containing CRE1 and CRE2 were responsive to the ISO/IBMX treatment (Fig. 4C). To determine the responsible motif(s) for this trans-activation of the *Fgf23* gene promoter, we introduced mutations in CRE1 and/or CRE2 and found that CRE2 was responsible for ISO/IBMX-induced activation of the *Fgf23* gene promoter (Fig. 4D).

Overexpression of Cry1 Blunted the Effects of ISO on *Fgf23* Induction in UMR-106 Cells—These findings may support the concept that *Fgf23* expression is regulated by sympathetic activity, but it is still unclear as to why *Fgf23* induction by ISO is regulated in a time-dependent manner *in vivo*. To solve this issue, we assessed whether Cry1 was involved in the ISO-induced activation of *Fgf23* expression because Cry1 has been implicated in the suppression of ISO-induced cAMP accumulation in HEK293 cells (36). Indeed, ISO-induced *Fgf23* expression was evident when Cry1 expression was low in the femur (Figs. 1C and 3C). Based on these results, we tested our hypothesis that Cry1 suppressed ISO-induced *Fgf23* induction by blocking CREB signaling in osteoblastic cells. To test this hypothesis, we overexpressed Cry1 in UMR-106 cells and investigated the effect of ISO on the phosphorylation of CREB. As shown in Fig. 5A, the ISO-induced phosphorylation of CREB was impaired in Cry1-overexpressing cells compared with GFP-expressing control cells. In line with this, ISO-induced trans-activation of the *Fgf23* promoter was decreased in cells overexpressing Cry1 (Fig. 5B). To further determine the role of

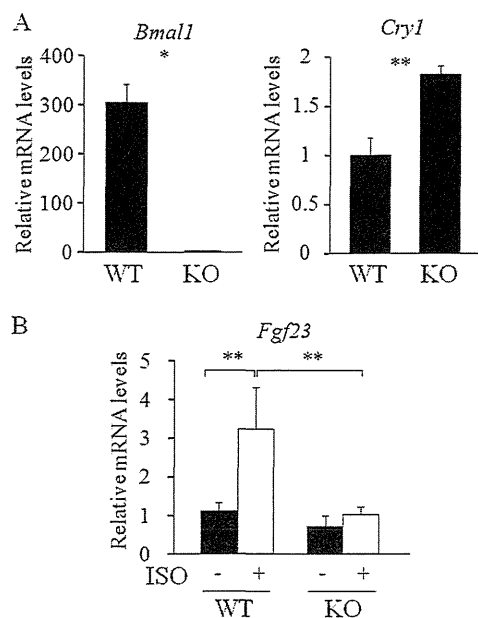


FIGURE 6. *Fgf23* induction by the ISO treatment in the femur was impaired in *Bmal1*-deficient mice. *A*, the expression of *Bmal1* and *Cry1* was determined by real-time RT-PCR in the femur collected from WT mice and *Bmal1*-deficient mice at ZT16 ($n = 3-5$). *B*, WT mice and *Bmal1*-deficient mice were fed a control diet for 2 weeks from 8 weeks of age, and ISO was injected intraperitoneally at ZT12. Four h after the injection, the expression of *Fgf23* in the femur was analyzed by real-time RT-PCR ($n = 4-5$). Values are expressed as the mean \pm S.E. (error bars). *, $p < 0.01$; **, $p < 0.05$.

the circadian clock network in ISO-induced *Fgf23* induction, we utilized *Bmal1*-deficient mice in which *Cry1* expression was higher than that in WT littermate controls (Fig. 6A). The administration of ISO at ZT12 showed a significant increase in *Fgf23* expression in the femur of WT mice, whereas the induction of *Fgf23* was weaker in the femur of *Bmal1*-deficient mice (Fig. 6B).

Parathyroid Hormone Induced *Fgf23* Expression When Administered at ZT12—Because PTH has been shown to activate the CREB pathway and induce *Fgf23* expression (4, 37), we next tested whether the PTH-induced activation of *Fgf23* was also regulated in a circadian rhythm-dependent manner. To test this hypothesis, we administered PTH(1-34) intraperitoneally to WT mice at ZT0 or ZT12. Four h after the injection, the expression of *Fgf23* was analyzed in the femur. The skeletal expression of *Fgf23* exhibited a significant response to PTH when injected at ZT12, which was associated with a trend toward an increased expression of *Rankl* and a decreased expression of *Sost*, known to be regulated by PTH activation in osteoblastic cells (38), whereas PTH had no effect on *Fgf23* expression when injected at ZT0 (Fig. 7). These results suggest the possibility of the circadian regulation of PTH action with respect to *Fgf23* induction in the skeleton.

***Fgf23* Induction by Dietary Phosphate Load Was Not Likely Caused by Sympathetic Activation**—Because it is still unclear as to whether circadian *Fgf23* expression is regulated by food intake itself or the influx of phosphate from the diet, we finally tested whether sympathetic activity was involved in *Fgf23* induction by dietary phosphate load. For this purpose, WT mice were fed either a control diet or high phosphate diet for 2 weeks in the presence or absence of PRO. Ingesting the high

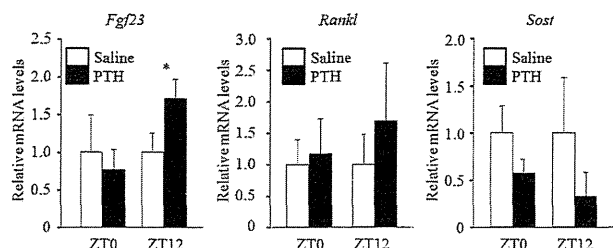


FIGURE 7. PTH induced skeletal *Fgf23* expression in a circadian fashion. PTH was intraperitoneally administered in WT mice at ZT0 or ZT12, and samples were collected 4 h after the injection. The expression of *Fgf23*, *Rankl*, and *Sost* in the femur was determined using real-time RT-PCR ($n = 3-6$). Values are expressed as the mean \pm S.E. (error bars). *, $p < 0.05$.

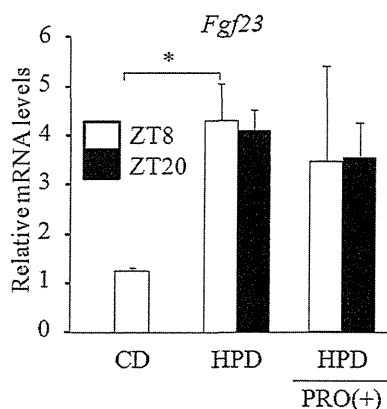


FIGURE 8. Propranolol did not affect skeletal *Fgf23* expression induced by dietary phosphate load. WT mice were fed either control diet (CD) or high phosphate diet (HPD) for 2 weeks from 8 weeks of age in the presence or absence of PRO in the drinking water. The expression of *Fgf23* in the femur was determined using real-time RT-PCR ($n = 3-5$). Values are expressed as the mean \pm S.E. (error bars). *, $p < 0.01$.

phosphate diet caused a significant elevation in *Fgf23* expression in the femur (Fig. 8), but the concomitant administration of PRO did not affect the levels of *Fgf23* expression in the femur (Fig. 8), which indicates that the timing of food intake, and not the amount of ingested phosphate, may determine the circadian profiles of skeletal *Fgf23* expression.

The Increase in Skeletal *Fgf23* Expression during DP Was Associated with Elevated FGF23 Levels in Serum and Enhanced Phosphate Excretion in the Urine—We finally investigated the association between the increase in skeletal *Fgf23* expression during DP and systemic phosphate metabolism. Consistent with the rhythmic expression pattern of skeletal *Fgf23*, total FGF23 levels in the serum exhibited a circadian expression profile with peak levels at ZT 16 (Fig. 9A). Circulating biologically active (intact) FGF23 levels also showed greater levels during DP with the highest at ZT20 compared with ZT0 (Fig. 9B). In line with the increased serum FGF23 levels during DP, expression of *Slc34a1* and *Slc34a3* coding for $\text{NaP}_i\text{-IIa}$ and $\text{NaP}_i\text{-IIc}$, respectively, showed decreased expressions during DP (Fig. 9, C and D, and supplemental Fig. S1), suggesting the enhanced phosphate excretion in the urine during this period. Indeed, serum phosphate concentrations showed a decline during DP associated with enhanced phosphate excretion in the urine (Fig. 9, E and F). We also analyzed the expression profile of *Cyp27b1* and *Cyp24a1*, other target genes of FGF23 signaling in the kidney, and found that these genes exhibited circadian profiles (Fig. 10). The expression of *Cyp27b1*, which was down-regu-

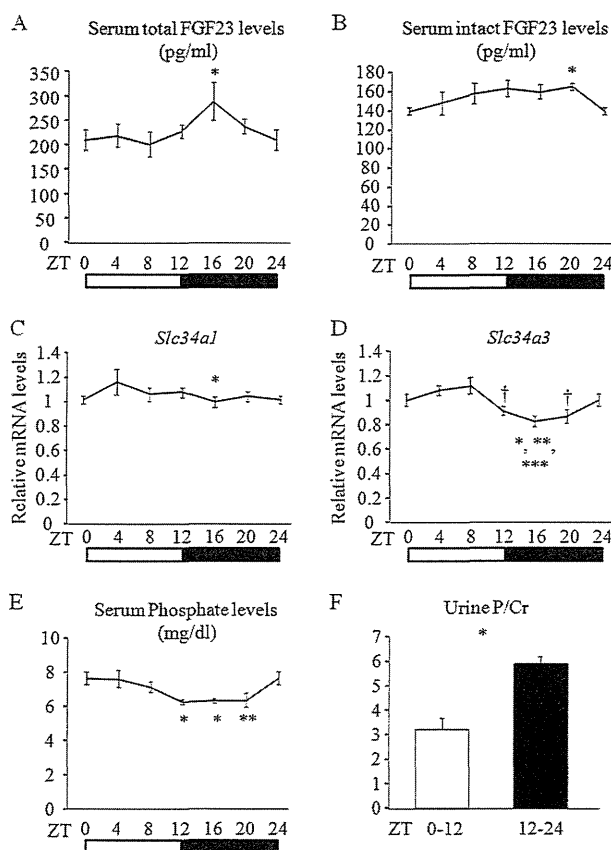


FIGURE 9. Increase in skeletal *Fgf23* expression during the dark phase was associated with elevated circulating FGF23 levels and enhanced phosphate excretion in the urine. WT mice were maintained under a light-dark regimen (12-h:12-h cycle) and fed *ad libitum*. Samples were collected every 4 h from ZT0. A and B, serum concentrations of total (C terminus) FGF23 ($n = 6-7$, *, $p < 0.05$ versus ZT0 and ZT8) (A) and intact (full-length) FGF23 ($n = 6-7$, *, $p < 0.05$ versus ZT0) (B) were measured. C and D, the expression of *slc34a1* ($n = 6-7$, *, $p < 0.05$ versus ZT4) (C) and *slc34a3* ($n = 6-7$, *, $p < 0.001$ versus ZT8; **, $p < 0.01$ versus ZT4; ***, $p < 0.05$ versus ZT0; †, $p < 0.05$ versus ZT4 and ZT8) (D) in the kidney was determined by real-time RT-PCR. E, serum concentration of phosphate was measured ($n = 7$, *, $p < 0.01$ versus ZT0; **, $p < 0.05$ versus ZT0). F, urine was collected either during the light phase (ZT0–12) or dark phase (ZT12–24), and phosphate and creatinine (Cr) levels in the urine were measured ($n = 9$, *, $p < 0.001$). The white bar and black bar represent the light phase and dark phase, respectively. Values are expressed as the mean \pm S.E. (error bars).

lated by FGF23 activation, was lower during the DP when FGF23 levels were greater, but the circadian profile of *Cyp24a1*, which was up-regulated by FGF23 activation, did not show any association with that of FGF23, suggesting that circadian profile of genes involved in vitamin D metabolism is mainly regulated by the circadian network independent of circadian FGF23 profiles.

DISCUSSION

In the present study, we demonstrated that skeletal *Fgf23* expression possessed a circadian expression profile. Importantly, the peak in skeletal *Fgf23* expression shifted when mice were maintained under LP-RF regimen, suggesting that timing of food intake is an important determinant for rhythmic expression profile of skeletal *Fgf23*. To investigate the mechanism responsible for generating the rhythmicity in skeletal *Fgf23* expression, we had a hypothesis that sympathetic activity may be the responsible factor linking food intake and skeletal

FGF23 and Circadian Clock Network

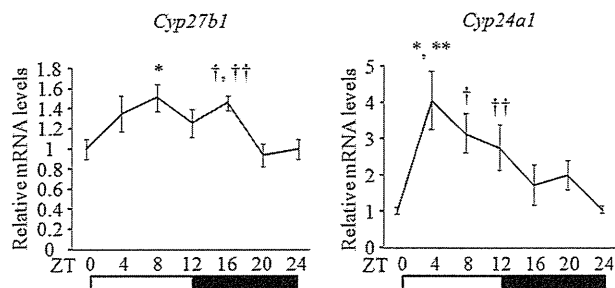


FIGURE 10. Circadian expression profiles of genes involved in vitamin D metabolism in the kidney. WT mice were maintained under a light-dark regimen (12-h:12-h cycle) and fed *ad libitum*. Samples were collected every 4 h from ZT0. The expression of *Cyp27b1* ($n = 8-10$, *, $p < 0.01$ versus ZT0 and ZT20; †, $p < 0.01$ versus ZT20; ††, $p < 0.05$ versus ZT0) and *Cyp24a1* ($n = 9-10$, *, $p < 0.001$ versus ZT0; **, $p < 0.01$ versus ZT16 and ZT20; †, $p < 0.01$ versus ZT0; ††, $p < 0.05$ versus ZT0) in the kidney was determined by real-time RT-PCR. The white bar and black bar represent the light phase and dark phase, respectively. Values are expressed as the mean \pm S.E. (error bars).

Fgf23 expression based on the previous findings that sympathetic activation has been shown to be associated with food intake (28) and display a circadian profile with greater levels during the DP when food intake is active in mice (34). Indeed, we found that the administration of ISO caused an elevation in skeletal *Fgf23* expression in a circadian rhythm-dependent manner. Furthermore, the blockade of sympathetic activity by PRO in mice under LP-RF conditions altered the circadian *Fgf23* expression profile such that the peak expression of *Fgf23* was not observed. Importantly, LP-RF caused a phase shift in sympathetic activity with greater levels during the LF. These results imply that sympathetic activation driven by food intake is a positive regulator for skeletal *Fgf23* expression.

One of the important issues to be addressed is the effect of circadian regulation of skeletal *Fgf23* expression on systemic phosphate metabolism. To address this issue we performed series of analyses and found that circulating both total and biologically active (intact) FGF23 levels were greater during DP. In line with the increase in FGF23 levels during DP, the expression of *slc34a1* and *slc34a3*, known to be down-regulated by FGF23 activation in the kidney, was decreased during this period associated with enhanced phosphate excretion in the urine and decreased phosphate levels in the serum. Because food intake is increased at the beginning of DP in mice, these findings may suggest that the increase in skeletal *Fgf23* expression during DP has an important role in handling the phosphate influx from the diet. It is important to note that the amplitude of circadian profile of intact FGF23 levels is not as obvious as that of total FGF23 levels, suggesting the possibility of the existence of additional mechanism regulating circadian profile of intact FGF23 in the circulation. Because FGF23 protein is known to be cleaved between Arg-179 and Ser-180 (39), it is possible that the post-translational modification or processing of FGF23 protein may create the difference in amplitude between total and intact FGF23 circadian rhythms, although the mechanisms of how FGF23 is cleaved in the circulation are not well defined and still need to be determined. Thus, these lines of evidence may imply that the circadian clock network may function in a coordinated manner involving multiple organs to maintain systemic phosphate homeostasis.

The present findings demonstrate that the timing of food intake regulates the circadian profile of skeletal *Fgf23* expression, but it is still unclear as to whether circadian *Fgf23* expression is regulated by the influx of phosphate from the diet. Because inorganic phosphate has been shown to induce *Fgf23* expression in osteocyte-like IDG-SW3 cells (40), it is possible that the influx of phosphate from the diet may regulate circadian *Fgf23* expression; however, previous *in vivo* studies failed to demonstrate an acute effect of dietary phosphate on FGF23 induction (41, 42), making this concept unlikely to be operative. Despite the lack of an increase in FGF23 levels in response to an acute phosphate load, it has been well established that a chronic phosphate load causes elevations in FGF23 levels (43). Consistent with previous reports, we detected a significant increase in skeletal *Fgf23* expression in mice fed a high phosphate diet, but this increase was not associated with sympathetic activation because the concomitant administration of PRO did not affect *Fgf23* expression. These findings may indicate that the timing of food intake, and not the amount of ingested phosphate, is a predominant determinant for the circadian profiles of skeletal *Fgf23* expression.

The involvement of Cry1 in the regulation of G protein-coupled receptor signaling pathways has been demonstrated previously in a mouse model in which CRE activated luciferase activity in the liver (36). In these mice luciferase activity in the liver was markedly higher at ZT13 than at ZT1, which was associated with increased CREB phosphorylation, and was inhibited when Cry1 was overexpressed (36). The underlying mechanisms described in this study included the suppression of cAMP accumulation by binding of Cry1 to $G_s\alpha$ proteins (36). Based on these previous findings, we investigated whether a similar mechanism was operative in osteoblastic cells and found that overexpression of Cry1 suppressed ISO-induced CREB phosphorylation and trans-activation of the *Fgf23* promoter in osteoblastic UMR-106 cells, which indicated that Cry1 also suppressed ISO-induced *Fgf23* expression in osteoblastic cells. CREB has been shown to bind to the palindromic sequence (TGACGTCA) called CRE with strong affinity and regulate the transcription of target genes. In addition to this canonical CRE, CREB has also been shown to bind to CRE variants albeit with low affinity (44). The sequence of CRE detected in this study is one such variant that is known to mediate CREB signaling (44), and this may be one of the reasons why the induction of luciferase activity by ISO was not intense. Because *in vivo* analysis revealed a significant increase in *Fgf23* expression by the ISO treatment, other CRE motif(s) may be present in other regions and affect the *in vivo* expression of *Fgf23*.

The regulation of *Fgf23* expression in bone has also been implicated in the action of PTH. For example, circulating FGF23 levels were shown to be elevated under conditions in which PTH signaling was continuously active such as chronic kidney disease and Jansen metaphyseal chondrodysplasia caused by a mutation in the *PTH1R* gene, which suggests that PTH is a positive regulator for *Fgf23* expression (37, 45). However, the negative action of PTH on *Fgf23* expression has also been demonstrated in a mouse model in which PTH was intermittently administered (46). Thus, the effect of PTH on *Fgf23* expression is context-specific and controversial (37, 45-47).

Hence, the result showing that the induction of skeletal *Fgf23* by a single injection of PTH was observed in a circadian manner may provide a clue to solve this controversial issue of PTH action on *Fgf23* expression although further studies are needed to precisely determine PTH action on *Fgf23* regulation.

In conclusion, in the present study we have provided evidence that the time of food intake determined the circadian profile of skeletal *Fgf23* expression which involved a systemic activation of sympathetic tone and that sympathetic activation was peripherally regulated by *Cry1* expression in the skeleton. Given the paucity of data as to the mechanisms regulating skeletal *Fgf23* expression, these lines of evidence may shed light on new regulatory networks of FGF23 which could be important for understanding the physiology of phosphate metabolism.

Acknowledgments—We thank Yasuhisa Ohata, Jin Nishino, Miwa Yamazaki, and Kanako Tachikawa (Osaka Medical Center and Research Institute for Maternal and Child Health) for critical discussions.

REFERENCES

1. Bergwitz, C., and Jüppner, H. (2011) Phosphate sensing. *Adv. Chronic Kidney Dis.* **18**, 132–144
2. Razzaque, M. S. (2012) The role of Klotho in energy metabolism. *Nat. Rev. Endocrinol.* **8**, 579–587
3. Hubbard, S. R., and Till, J. H. (2000) Protein-tyrosine kinase structure and function. *Annu. Rev. Biochem.* **69**, 373–398
4. Quarles, L. D. (2012) Skeletal secretion of FGF-23 regulates phosphate and vitamin D metabolism. *Nat. Rev. Endocrinol.* **8**, 276–286
5. Martin, A., David, V., and Quarles, L. D. (2012) Regulation and function of the FGF23/Klotho endocrine pathways. *Physiol. Rev.* **92**, 131–155
6. Shimada, T., Kakitani, M., Yamazaki, Y., Hasegawa, H., Takeuchi, Y., Fujita, T., Fukumoto, S., Tomizuka, K., and Yamashita, T. (2004) Targeted ablation of *Fgf23* demonstrates an essential physiological role of FGF23 in phosphate and vitamin D metabolism. *J. Clin. Invest.* **113**, 561–568
7. Urakawa, I., Yamazaki, Y., Shimada, T., Iijima, K., Hasegawa, H., Okawa, K., Fujita, T., Fukumoto, S., and Yamashita, T. (2006) Klotho converts canonical FGF receptor into a specific receptor for FGF23. *Nature* **444**, 770–774
8. Kuro-o, M., Matsumura, Y., Aizawa, H., Kawaguchi, H., Suga, T., Utsugi, T., Ohyama, Y., Kurabayashi, M., Kaname, T., Kume, E., Iwasaki, H., Iida, A., Shiraki-Iida, T., Nishikawa, S., Nagai, R., and Nabeshima, Y. I. (1997) Mutation of the mouse *klotho* gene leads to a syndrome resembling ageing. *Nature* **390**, 45–51
9. Kurosu, H., Ogawa, Y., Miyoshi, M., Yamamoto, M., Nandi, A., Rosenblatt, K. P., Baum, M. G., Schiavi, S., Hu, M. C., Moe, O. W., and Kuro-o, M. (2006) Regulation of fibroblast growth factor-23 signaling by Klotho. *J. Biol. Chem.* **281**, 6120–6123
10. ADHR Consortium. (2000) Autosomal dominant hypophosphataemic rickets is associated with mutations in FGF23. *Nat. Genet.* **26**, 345–348
11. Feng, J. Q., Ward, L. M., Liu, S., Lu, Y., Xie, Y., Yuan, B., Yu, X., Rauch, F., Davis, S. I., Zhang, S., Rios, H., Drezner, M. K., Quarles, L. D., Bonewald, L. F., and White, K. E. (2006) Loss of DMP1 causes rickets and osteomalacia and identifies a role for osteocytes in mineral metabolism. *Nat. Genet.* **38**, 1310–1315
12. Lorenz-Depiereux, B., Schnabel, D., Tiosano, D., Häusler, G., and Strom, T. M. (2010) Loss-of-function *ENPP1* mutations cause both generalized arterial calcification of infancy and autosomal-recessive hypophosphatemic rickets. *Am. J. Hum. Genet.* **86**, 267–272
13. Liu, S., Tang, W., Zhou, J., Stubbs, J. R., Luo, Q., Pi, M., and Quarles, L. D. (2006) Fibroblast growth factor 23 is a counter-regulatory phosphaturic hormone for vitamin D. *J. Am. Soc. Nephrol.* **17**, 1305–1315
14. Shimada, T., Yamazaki, Y., Takahashi, M., Hasegawa, H., Urakawa, I., Oshima, T., Ono, K., Kakitani, M., Tomizuka, K., Fujita, T., Fukumoto, S., and Yamashita, T. (2005) Vitamin D receptor-independent FGF23 actions in regulating phosphate and vitamin D metabolism. *Am. J. Physiol. Renal Physiol.* **289**, F1088–F1095
15. Kolek, O. I., Hines, E. R., Jones, M. D., LeSueur, L. K., Lipko, M. A., Kiela, P. R., Collins, J. F., Haussler, M. R., and Ghishan, F. K. (2005) 1 α ,25-Dihydroxyvitamin D3 up-regulates FGF23 gene expression in bone: the final link in a renal-gastrointestinal-skeletal axis that controls phosphate transport. *Am. J. Physiol. Gastrointest. Liver Physiol.* **289**, G1036–G1042
16. Nelson, W. (1964) Aspects of circadian periodic changes in phosphorus metabolism in mice. *Am. J. Physiol.* **206**, 589–598
17. Carpenter, T. O., Insogna, K. L., Zhang, J. H., Ellis, B., Nieman, S., Simpson, C., Olear, E., and Gundberg, C. M. (2010) Circulating levels of soluble Klotho and FGF23 in X-linked hypophosphatemia: circadian variance, effects of treatment, and relationship to parathyroid status. *J. Clin. Endocrinol. Metab.* **95**, E352–E357
18. Smith, E. R., Cai, M. M., McMahon, L. P., and Holt, S. G. (2012) Biological variability of plasma intact and C-terminal FGF23 measurements. *J. Clin. Endocrinol. Metab.* **97**, 3357–3365
19. Vollmers, C., Gill, S., DiTacchio, L., Pulivarthy, S. R., Le, H. D., and Panda, S. (2009) Time of feeding and the intrinsic circadian clock drive rhythms in hepatic gene expression. *Proc. Natl. Acad. Sci. U.S.A.* **106**, 21453–21458
20. Green, C. B., Takahashi, J. S., and Bass, J. (2008) The meter of metabolism. *Cell* **134**, 728–742
21. Bass, J., and Takahashi, J. S. (2010) Circadian integration of metabolism and energetics. *Science* **330**, 1349–1354
22. Liu, C., Li, S., Liu, T., Borjigin, J., and Lin, J. D. (2007) Transcriptional coactivator PGC-1 α integrates the mammalian clock and energy metabolism. *Nature* **447**, 477–481
23. Damiola, F., Le Minh, N., Preitner, N., Kornmann, B., Fleury-Olela, F., and Schibler, U. (2000) Restricted feeding uncouples circadian oscillators in peripheral tissues from the central pacemaker in the suprachiasmatic nucleus. *Genes Dev.* **14**, 2950–2961
24. Zhang, L., Abraham, D., Lin, S. T., Oster, H., Eichele, G., Fu, Y. H., and Ptáček, L. J. (2012) PKC γ participates in food entrainment by regulating BMAL1. *Proc. Natl. Acad. Sci. U.S.A.* **109**, 20679–20684
25. Fagius, J., and Berne, C. (1994) Increase in muscle nerve sympathetic activity in humans after food intake. *Clin. Sci.* **86**, 159–167
26. Sakaguchi, T., Arase, K., Fisler, J. S., and Bray, G. A. (1988) Effect of starvation and food intake on sympathetic activity. *Am. J. Physiol.* **255**, R284–R288
27. Troisi, R. J., Weiss, S. T., Parker, D. R., Sparrow, D., Young, J. B., and Landsberg, L. (1991) Relation of obesity and diet to sympathetic nervous system activity. *Hypertension* **17**, 669–677
28. Tseng, Y. H., Cypess, A. M., and Kahn, C. R. (2010) Cellular bioenergetics as a target for obesity therapy. *Nat. Rev. Drug Discov.* **9**, 465–482
29. Ralph, M. R., Foster, R. G., Davis, F. C., and Menaker, M. (1990) Transplanted suprachiasmatic nucleus determines circadian period. *Science* **247**, 975–978
30. Kornmann, B., Schaad, O., Bujard, H., Takahashi, J. S., and Schibler, U. (2007) System-driven and oscillator-dependent circadian transcription in mice with a conditionally active liver clock. *PLoS Biol.* **5**, e34
31. Shimba, S., Ogawa, T., Hitosugi, S., Ichihashi, Y., Nakadaira, Y., Kobayashi, M., Tezuka, M., Kosuge, Y., Ishige, K., Ito, Y., Komiya, K., Okamoto-Ogura, Y., Kimura, K., and Saito, M. (2011) Deficient of a clock gene, brain and muscle Arnt-like protein-1 (BMAL1), induces dyslipidemia and ectopic fat formation. *PLoS One* **6**, e25231
32. Kondo, H., Nifuji, A., Takeda, S., Ezura, Y., Rittling, S. R., Denhardt, D. T., Nakashima, K., Karsenty, G., and Noda, M. (2005) Unloading induces osteoblastic cell suppression and osteoclastic cell activation to lead to bone loss via sympathetic nervous system. *J. Biol. Chem.* **280**, 30192–30200
33. Takeda, S., Eleftheriou, F., Levasseur, R., Liu, X., Zhao, L., Parker, K. L., Armstrong, D., Ducy, P., and Karsenty, G. (2002) Leptin regulates bone formation via the sympathetic nervous system. *Cell* **111**, 305–317
34. Fu, L., Patel, M. S., Bradley, A., Wagner, E. F., and Karsenty, G. (2005) The molecular clock mediates leptin-regulated bone formation. *Cell* **122**, 803–815
35. Eleftheriou, F., Ahn, J. D., Takeda, S., Starbuck, M., Yang, X., Liu, X., Kondo,

FGF23 and Circadian Clock Network

- H., Richards, W. G., Bannon, T. W., Noda, M., Clement, K., Vaisse, C., and Karsenty, G. (2005) Leptin regulation of bone resorption by the sympathetic nervous system and CART. *Nature* **434**, 514–520
36. Zhang, E. E., Liu, Y., Dentin, R., Pongsawakul, P. Y., Liu, A. C., Hirota, T., Nusinow, D. A., Sun, X., Landais, S., Kodama, Y., Brenner, D. A., Montminy, M., and Kay, S. A. (2010) Cryptochrome mediates circadian regulation of cAMP signaling and hepatic gluconeogenesis. *Nat. Med.* **16**, 1152–1156
37. Lavi-Moshayoff, V., Wasserman, G., Meir, T., Silver, J., and Naveh-Many, T. (2010) PTH increases *FGF23* gene expression and mediates the high-*FGF23* levels of experimental kidney failure: a bone parathyroid feedback loop. *Am. J. Physiol. Renal Physiol.* **299**, F882–F889
38. Keller, H., and Kneissel, M. (2005) *SOST* is a target gene for PTH in bone. *Bone* **37**, 148–158
39. Benet-Pagès, A., Lorenz-Depiereux, B., Zischka, H., White, K. E., Econs, M. J., and Strom, T. M. (2004) *FGF23* is processed by proprotein convertases but not by PHEX. *Bone* **35**, 455–462
40. Ito, N., Findlay, D. M., Anderson, P. H., Bonewald, L. F., and Atkins, G. J. (2013) Extracellular phosphate modulates the effect of $1\alpha,25$ -dihydroxy vitamin D3 ($1,25D$) on osteocyte like cells. *J. Steroid Biochem. Mol. Biol.* **136**, 183–186
41. Larsson, T., Nisbeth, U., Ljunggren, O., Jüppner, H., and Jonsson, K. B. (2003) Circulating concentration of FGF-23 increases as renal function declines in patients with chronic kidney disease, but does not change in response to variation in phosphate intake in healthy volunteers. *Kidney Int.* **64**, 2272–2279
42. Nishida, Y., Taketani, Y., Yamanaka-Okumura, H., Imamura, F., Taniguchi, A., Sato, T., Shuto, E., Nashiki, K., Arai, H., Yamamoto, H., and Takeda, E. (2006) Acute effect of oral phosphate loading on serum fibroblast growth factor 23 levels in healthy men. *Kidney Int.* **70**, 2141–2147
43. Perwad, F., Azam, N., Zhang, M. Y., Yamashita, T., Tenenhouse, H. S., and Portale, A. A. (2005) Dietary and serum phosphorus regulate fibroblast growth factor 23 expression and $1,25$ -dihydroxyvitamin D metabolism in mice. *Endocrinology* **146**, 5358–5364
44. Smith, B., Fang, H., Pan, Y., Walker, P. R., Famili, A. F., and Sikorska, M. (2007) Evolution of motif variants and positional bias of the cyclic-AMP response element. *BMC Evol. Biol.* **7**, S15
45. Brown, W. W., Jüppner, H., Langman, C. B., Price, H., Farrow, E. G., White, K. E., and McCormick, K. L. (2009) Hypophosphatemia with elevations in serum fibroblast growth factor 23 in a child with Jansen's metaphyseal chondrodysplasia. *J. Clin. Endocrinol. Metab.* **94**, 17–20
46. Samadfam, R., Richard, C., Nguyen-Yamamoto, L., Bolivar, I., and Goltzman, D. (2009) Bone formation regulates circulating concentrations of fibroblast growth factor 23. *Endocrinology* **150**, 4835–4845
47. Saji, F., Shigematsu, T., Sakaguchi, T., Ohya, M., Orita, H., Maeda, Y., Ooura, M., Mima, T., and Negi, S. (2010) Fibroblast growth factor 23 production in bone is directly regulated by $1\alpha,25$ -dihydroxyvitamin D, but not PTH. *Am. J. Physiol. Renal Physiol.* **299**, F1212–F1217

Overgrowth Syndrome Associated With a Gain-of-Function Mutation of the Natriuretic Peptide Receptor 2 (*NPR2*) Gene

Kohji Miura,¹ Ok-Hwa Kim,² Hey Ran Lee,³ Noriyuki Namba,¹ Toshimi Michigami,⁴ Won Joon Yoo,³ In Ho Choi,³ Keiichi Ozono,¹ and Tae-Joon Cho^{3*}

¹Department of Pediatrics, Osaka University Graduate School of Medicine, Osaka, Japan

²Department of Radiology, Ajou University Hospital, Suwon, Republic of Korea

³Division of Pediatric Orthopaedics, Seoul National University Children's Hospital, Seoul, Republic of Korea

⁴Department of Bone and Mineral Research, Osaka Medical Centre and Research Institute for Maternal and Child Health, Osaka, Japan

Manuscript Received: 11 March 2013; Manuscript Accepted: 8 August 2013

The signal pathway of the C-type natriuretic (CNP) and its receptor, natriuretic peptide receptor 2 (NPR2) is involved in the longitudinal growth of long bones. Loss of function mutations at NPR2 cause acromesomelic dysplasia, type Maroteaux, while overproduction of CNP by chromosomal translocation and a gain-of-function mutation at NPR2 have been reported to be responsible for an overgrowth syndrome in three cases and one family, respectively. We identified a four-generation family with an overgrowth syndrome characterized by tall stature, macrodactyly of the great toes, scoliosis, coxa valga and slipped capital femoral epiphysis, similar to those previously reported in association with CNP/NPR2 overactivity. The serum level of amino-terminal proCNP was normal in the proband. A novel missense mutation of *NPR2*, c.1462G>C (p.Ala488Pro) was found to cosegregate with the phenotype in this family. In vitro transfection assay of the mutant NPR2 revealed overactivity of the mutant receptor at baseline as well as with the ligand. This overgrowth syndrome caused by a gain-of-function mutation at *NPR2* should be differentiated from Marfan or related syndromes, and may be categorized along with the overgrowth syndrome caused by overproduction of CNP due to its phenotypical similarity as overgrowth CNP/NPR2 signalopathy. © 2013 Wiley Periodicals, Inc.

Key words: tall stature; CNP signal; scoliosis; macrodactyly of the big toe; slipped capital femoral epiphysis

INTRODUCTION

Natriuretic peptides are a family of hormones/paracrine factors regulating blood volume, blood pressure, ventricular hypertrophy, pulmonary hypertension, fat metabolism, and long bone growth [Potter et al., 2006]. They include atrial natriuretic peptide (ANP; OMIM 600296). CNP binds to a homodimeric transmembrane receptor, natriuretic peptide receptor B/guanylate cyclase B (NPR2; OMIM108961) to increase intracellular level of cyclic guanosine monophosphate (cGMP) [Schulz, 2005]. Several lines of evidence

How to Cite this Article:

Miura K, Kim O-H, Lee HR, Namba N, Michigami T, Yoo WJ, Choi IH, Ozono K, Cho T-J. 2014. Overgrowth syndrome associated with a gain-of-function mutation of the natriuretic peptide receptor 2 (NPR2) gene.

Am J Med Genet Part A 164A:156–163.

indicate that CNP-NPR2 signaling plays an important role in endochondral ossification [Yasoda et al., 1998; Teixeira et al., 2008]. Inactivation of CNP-NPR2 signaling resulted in dwarfism in both mouse and human. CNP knock-out mice (*Nppc*^{-/-}) or mice with homozygous loss-of-function mutations in *Npr2* result in undergrowth of the skeletal system [Chusho et al., 2001; Tsuji and Kunieda, 2005]. In humans, an autosomal recessive skeletal dysplasia, acromesomelic dysplasia, type Maroteaux (AMDM) characterized by disproportionately mesomelic shortening of the limbs and severe brachydactyly of the hands and feet is caused by homozygous or compound heterozygous loss-of-function mutations in *NPR2* [Bartels et al., 2004]. On the other hand, chronically elevated plasma level of CNP stimulates skeletal

Kohji Miura and Ok-Hwa Kim contributed equally to this work.

Grant sponsor: Ministry for Health, Welfare and Family Affairs Republic of Korea; Grant number: A080588; Grant sponsor: Ministry of Health, Labour and Welfare of Japan; Grant number: KH20Q007a-1.

*Correspondence to:

Tae-Joon Cho, M.D., Division of Pediatric Orthopaedics, Seoul National University Children's Hospital, 101 Daehang-ro Jongno-gu, Seoul 110-744, Republic of Korea.

E-mail: tjcho@snu.ac.kr

Article first published online in Wiley Online Library (wileyonlinelibrary.com): 20 November 2013

DOI 10.1002/ajmg.a.36218

growth in CNP-overproducing transgenic mice [Kake et al., 2009]. In humans, overproduction of CNP due to a chromosomal translocation causes an overgrowth syndrome [Bocciardi et al., 2007; Moncla et al., 2007]. A three-generation Japanese family was recently reported, with an overgrowth syndrome caused by a gain-of-function mutation in *NPR2* [Miura et al., 2012]. We identified and report a four-generation Korean family with similar phenotype and a novel gain-of-function mutation in *NPR2*.

MATERIALS AND METHODS

Clinical Report

This study was approved by the ethics committee at Seoul National University Hospital, and written informed consent was obtained from the proband and family members. An 8-year-old boy visited orthopedic clinic for awkward ambulation and ankle pain on walking. He was a product of normal full term pregnancy with a birth weight 3.2 kg and height 50 cm ($z = -0.04$). His macrodactyly of the big toe was observed since birth, something familiar to his family (Figs. 1 and 2). Developmental milestones were within normal limits. He was recognized as bigger than his age group after the neonatal period. On physical examination at 8 years of age, the height was 145 cm ($z = +3.67$), and weight was 40 kg (>97 th centile). He had Marfanoid habitus and arachnodactyly. Neurologic examination was free of abnormal findings. At age 12 years, an unstable slipped capital femoral epiphysis (SCFE) developed on the left hip. Physical examination at this age revealed height 183 cm ($z = +5.19$), weight 71 kg (>97 th centile), BMI 21.2 kg/m². He showed long and slender fingers and toes, the hallux being remarkably longer than the other toes, ankle valgus deformity, and scoliosis. No anomalies of cardiac valves or the aorta were found on echocardiogram. Blood pressure was within normal limits. No abnormality was observed in ophthalmic and otologic examinations. Hematological, biochemical and endocrinological

values including insulin-like growth factor-I (IGF-I) were within normal ranges. However, bone formation and resorption markers were increased—osteocalcin, 118 ng/ml (reference range, 8–50); urinary cross-linked N-telopeptide of type I collagen, 969 BCE/mM creatinine (reference range, 21–83). Bone mineral density of L2-4 as measure by dual energy X-ray absorptiometry (Lunar Prodigy Advance, GE Healthcare, Waukesha, WI) was 0.791g/cm² ($z = -0.3$). Considering the tall stature of this patient, this BMD result may suggest presence of more severe osteopenia. Radiological survey of the skeleton showed coxa valga deformity of the femora, slipped capital femoral epiphysis, and lumbar scoliosis (Fig. 3). Arachnodactyly of all fingers and toes; of these, disproportionately long and large great toes were observed. Investigation of the family history revealed a four-generation family with 11 family members including the proband that could be considered to have the same phenotype. Five of 11 affected members were examined. They were characterized by tall stature (exceeded +4 SD compared to age matched control height of Korean population) and markedly long big toes. All of them showed coxa valga deformity with epiphyseal dysplasia of the femoral capital epiphyses and two had SCFE (Fig. 4). Three of them had lumbar scoliosis. The vertebral bodies were tall and showing endplate irregularities and narrowing of the intervertebral disc spaces in four of them. As seen in the clinical phenotype, radiograph of the feet showed extremely elongated metatarsals and assorted phalanges of the great toe symmetrically. The hands of all affected individuals showed arachnodactyly without elongation of specific fingers.

Mutation Analysis

Genomic DNA was extracted from the circulating leukocytes from the proband and family members available (Fig. 1). All the exons of *CNP*, *NPR2*, Natriuretic peptide receptor C (*NPR3*; MIM108962), and fibroblast growth factor receptor 3 (*FGFR3*; MIM134934) were

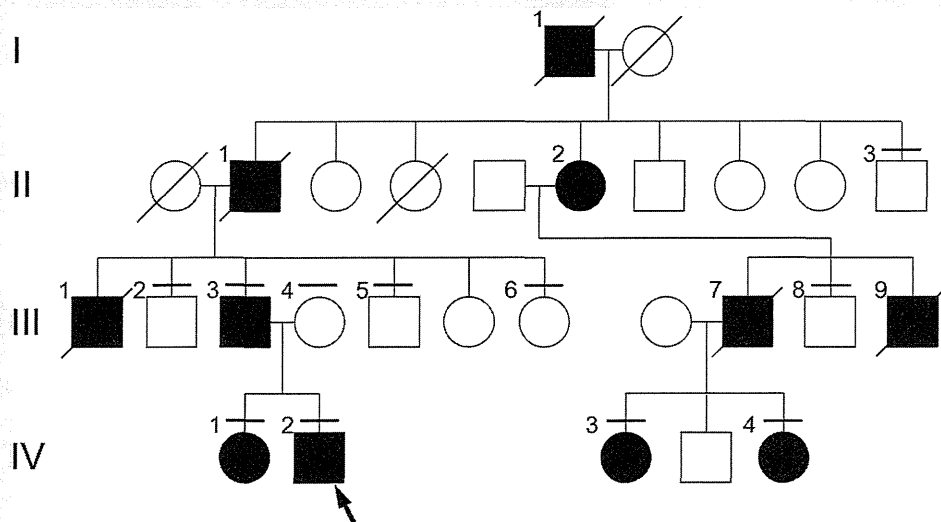


FIG. 1. Pedigree of the family. There are several father-to-son transmissions of the phenotype, revealing autosomal dominant inheritance pattern. Transverse bars above the circles or rectangles denote those who underwent mutation study. An arrow indicates the proband.

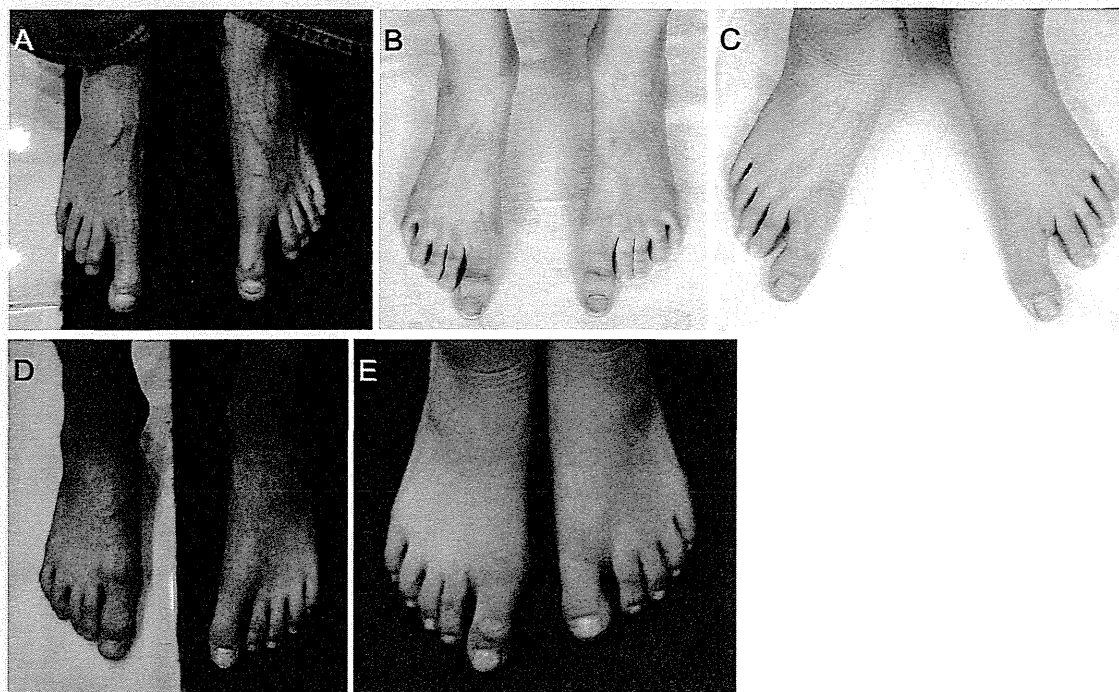


FIG. 2. Photographs of the feet of the affected family members. A: III-3, [B] IV-1, [C] IV-2, [D] IV-3, [E] IV-4. Patients IV-3 and IV-4 show relatively mild macrodactyly of the big toes as compared with the others.

amplified using specific primers [Miura et al., 2012] flanking the intron–exon boundaries according to published human genomic DNA sequences (UCSC genome browser: uc002vsl.1 at chromosome 2, 232498379–232499203; uc003zyd.1 at chromosome 9, 35782406–35799728; uc003jhv.2 at chromosome 5, 32711665–32787252; uc003gds.2 at chromosome 4, 1764337–1780396, respectively). Polymerase chain reaction (PCR) products were sequenced using a Big Dye terminator cycle sequencing kit (version 3.1; Applied Biosystems, Foster City, CA) and an ABI 3130 automated sequencer (Applied Biosystems).

Measurement of Serum Amino-Terminal (NT) proCNP Concentrations

Serum of IV-2 and III-3 were separated and collected, and NT-proCNP was assayed using an enzyme immunoassay (BIOMED-ICA, Vienna, Austria) according to the instructions provided. As a control, samples from eight healthy Japanese teenager boys and five women were also measured.

In Vitro Transfection Assay of Mutant NPR2

The pcDNA3.1(+)/hemagglutinin (HA)-tagged human NPR2 wild-type vector (HA-WT) was a gift from Dr. Yoshihiro Ogawa (Tokyo Medical and Dental University, Japan) [Hachiya et al., 2007]. The construct encoding the mutant p.Ala488Pro,

pcDNA3.1(+)/HA-human NPR-2 Ala488Pro (HA-Ala488Pro), was generated by PCR-based mutagenesis using HA-WT as the template, and primers containing the nucleotide change. All vector constructs were verified by bidirectional DNA sequencing.

HEK293A cells at confluence were transfected with empty vector containing green fluorescent protein (GFP), HA-WT, and HA-Ala488Pro using the liposomal transfection reagent FuGENE6 (Reagent: DNA = 3 μ l: 0.5 μ g, Roche, Indianapolis, IN, 12-well plate), according to the manufacturer's instructions. In 48 hr, cell lysate was harvested and immunoblot was performed to compare the expression of transfected genes, using a mouse monoclonal antibody against HA-tag (6E2, 1:1,000; Cell Signaling Technology, Boston, MA) as the primary antibody. As an internal control, β -actin in each sample was detected with a monoclonal anti- β -actin antibody (1:5,000; SIGMA-ALDRICH, Saint Louis, MO).

Transfected cells were serum-starved for 24 hr before the cGMP assay and then incubated at 37°C with 5% CO₂ in DMEM containing 0.5 mM IBMX (3-isobutyl-1-methylxanthine) (Wako, Osaka, Japan) for 10 min. The cells were next treated with vehicle (water) or 1 \times 10⁻⁷ M CNP-22 (Biochem Life Sciences, New Delhi, India) and incubated for another 10 min. The reaction was terminated with 300 μ l of 0.1 M HCl, and the cGMP concentration was measured by a competitive enzyme immunoassay (Cayman Chemical, Ann Arbor, MI). Results are presented as the mean \pm SD. Student's *t* test was used for statistical analyses.

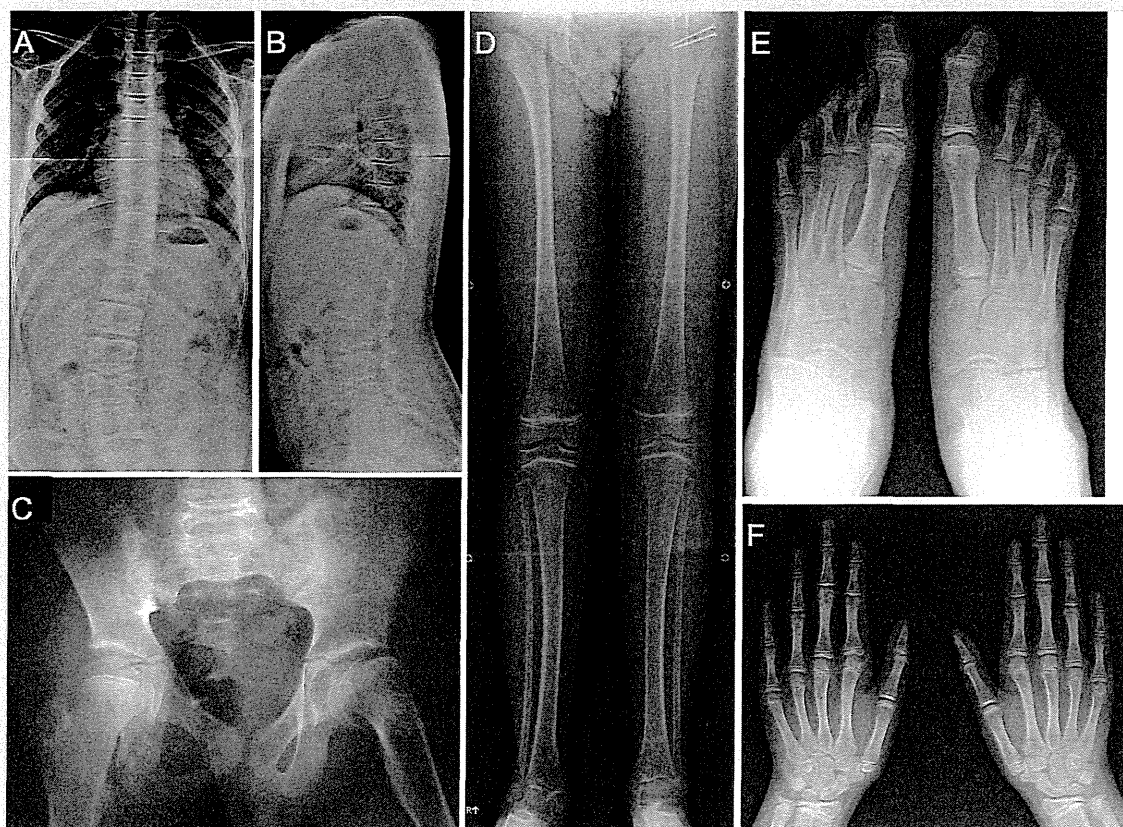


FIG. 3. Skeletal survey of the proband at age 12 years. A,B: Anteroposterior and lateral spine show lumbar scoliosis, slightly tall vertebral bodies with irregular end-plates, and narrowing of the intervertebral disc spaces. C: Pelvis shows coxa valga deformity and slipped femoral capital epiphysis on the left hip. D: Lower extremity demonstrates long and slender long bones with thin cortices. Mild inward bowing of the tibial and fibular diaphysis and ankle valgus deformity are noted. E: Feet show exceedingly long and large metatarsals and phalanges of the great toes symmetrically. F: Hands show overall arachnodactyly without specific digit elongation. Carpal bone age is advanced, measuring approximately 14 years of age.

RESULTS

Identification of a Novel Missense Mutation p.Ala488Pro in *NPR2*

On screening the sequences of exons of *CNP*, *NPR2*, *NPR3*, and *FGFR3* in the proband and family members as depicted on Figure 1, we identified a novel heterozygous sequence variation c. 1462G>C at *NPR2* in those who shared the similar phenotype (III-3, IV-1, IV-2, IV-3, and IV-4), but not in the remaining unaffected family members. The sequence variation eliminates an *NheI* cleavage site. PCR product of wild type containing this site (484 bp) would be cut into 95 and 389 bp fragments. Hence, these PCR products from all the patients tested were incubated with *NheI* (New England BioLabs, Ipswich, MA) overnight and run on an agarose gel to confirm the presence of this sequence variation. It showed that this sequence variation perfectly co-segregated with the phenotype in this family. It was predicted to substitute alanine for proline (p.Ala488Pro). This variant was not registered in the dbSNP (build 137) (<http://www.ncbi.nlm.nih.gov/projects/SNP/>) nor in the

NHLBI Exome Sequencing Project (ESP) (<http://evs.gs.washington.edu/EVS/>). It was not found in 400 alleles from healthy Korean or Japanese controls, either. Amino acid Ala488 is located in a highly conserved region of the juxtamembranous cytoplasmic domain of *NPR2* and is conserved across species (Fig. 5). No mutations were found in *CNP*, *NPR3*, or *FGFR3*.

CNP Was Not Overproduced in the Proband

Serum NT-proCNP levels of the proband (IV-2) and his mother were measured 9.68 and 2.65 pmol/L, respectively. Those of eight Japanese teenager boys of age ranging from 12 to 14 years averaged 6.0 ± 3.4 pmol/L (mean \pm standard deviation), and of five Japanese female adults of age ranging from 32 to 48 averaged 4.0 ± 0.9 pmol/L (unpublished data).

p.Ala488Pro Is a Gain-of-Function Mutation

To investigate the pathogenic significance of the p.Ala488Pro mutation, an in vitro functional assay was performed. HEK293A

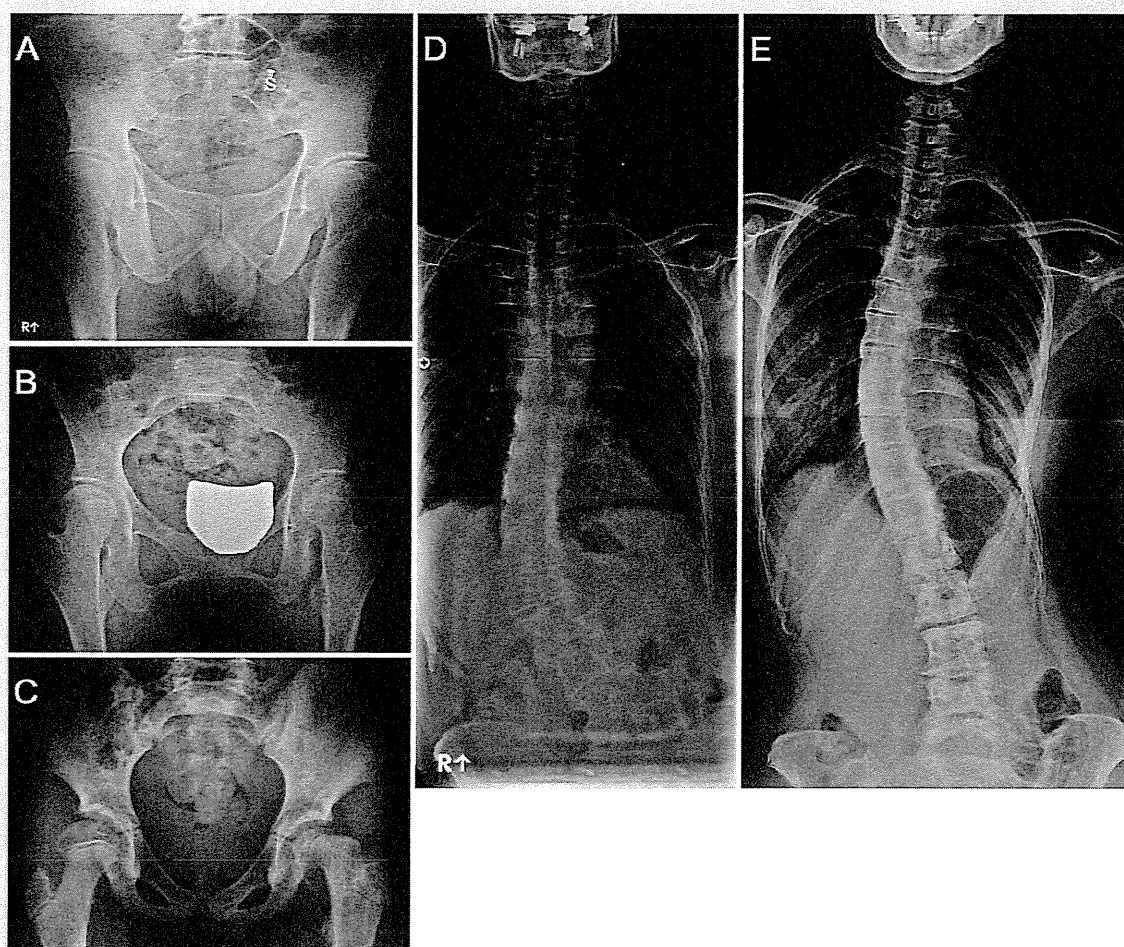


FIG. 4. Radiographs of the pelvis and spine of the other affected family members. Marked coxa valga deformity and residual valgus slipped capital femoral epiphysis are seen in Patients III-3 [A] and IV-1 [B]. C: Coxa valga deformity and unstable aggravation of the slipped capital femoral epiphysis at the left hip are seen in Patient IV-3 at age 11 years. D: Patient III-3 and [E] Patient IV-1 show thoracolumbar scoliosis. The vertebral bodies are tall and narrowing of the disc spaces is noted.

cells were transfected with the GFP, HA-WT, and HA-Ala488Pro. The Western blot analysis using anti-HA antibody confirmed that HA-WT and HA-Ala488Pro were expressed at comparable levels, with an approximate molecular size of 120 kDa (Fig. 6A). cGMP production in the cells expressing HA-WT, and HA-Ala488Pro was also examined. cGMP was produced in Ala488Pro-expressing cells, even in the absence of CNP, while no production was observed in HA-WT-expressing cells. Treatment with CNP-22 at a dose of 1×10^{-7} M increased intracellular cGMP levels with concentrations significantly higher in HA-Ala488Pro than in HA-WT-expressing cells (Fig. 6B). These results indicate that p.Ala488Pro is a gain-of-function type mutation.

DISCUSSION

The CNP/NPR2 signal pathway is involved in the longitudinal growth of skeletal system [Yasoda et al., 1998; Chusho et al., 2001;

Bartels et al., 2004; Tsuji and Kunieda, 2005; Bocciardi et al., 2007; Moncla et al., 2007; Teixeira et al., 2008; Kake et al., 2009]. Miura et al. [2012] reported a Japanese family with an overgrowth syndrome caused by a gain-of-function mutation at *NPR2*. The current study reports a second family showing a similar phenotype inherited as an autosomal dominant trait. The affected family members harbor a novel gain-of-function mutation at *NPR2*, c.1462G>C (p.Ala488Pro).

The mutation of the current family is located at a topological domain between transmembrane and protein kinase domains [UniProtKB[Internet]], while the previously reported gain-of-function mutation was at the guanylate cyclase domain [Miura et al., 2012]. Although the current mutation does not exist at the guanylate cyclase domain, it must bring conformational change at the 3D structure of guanylate cyclase domain to enhance its enzymatic activity with or without binding the ligand.

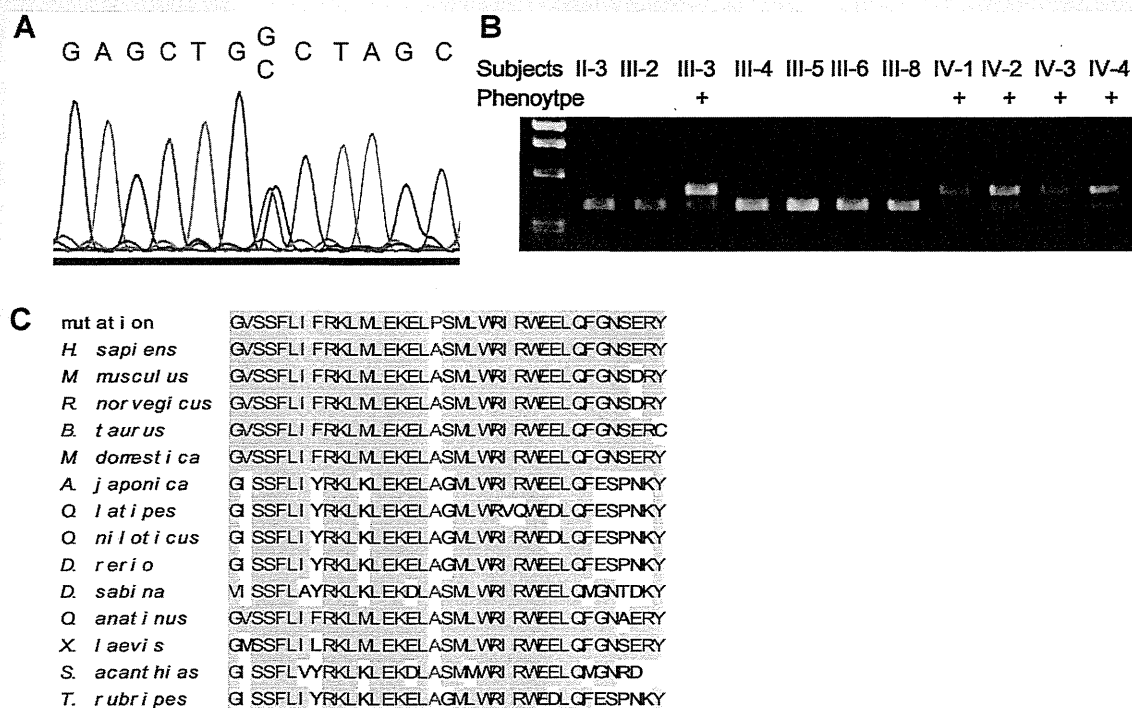


FIG. 5. Identification of the *Npr2* mutation. Sanger sequencing of the *NPR2* revealed a novel G → C missense mutation at nucleotide +1,462 creates a substitution, proline for alanine, at codon 488 in a heterozygous state. Among the subjects tested, this mutation was present in all the patients having the phenotype, and absent in all those who did not (A). This mutation eliminated the cleavage site of *NheI*, producing two bands on gel electrophoresis when treated with *NheI* (B). Amino acid alignment of *NPR2* among various species. Alanine at codon 488 is located in a highly conserved cytoplasmic region between the transmembrane and protein kinase domains of *NPR2* (C).

NPR2 is an interesting example of phenotypes contrasting between gain-of-function versus loss-of-function mutations at a gene encoding a receptor protein. Homozygous or compound heterozygous loss-of-function mutations of *NPR2* in humans cause a specific skeletal dysplasia, AMDM, characterized by marked short stature as well as short fingers and toes. The overgrowth syndrome by gain-of-function mutation seems to have phenotype opposite to that of AMDM. It is also interesting to note that the increased *NPR2* activity did not suppress CNP production, maintaining its serum level within normal limit. The same unsuppressed CNP production was also observed in the previous cases of gain-of-function mutation at *NPR2* [Miura et al., 2012], suggesting lack of feedback loop between the *NPR2* activity and CNP production.

This family has noticed 11 affected members by tall stature and long big toes through four generations. Neither macrodactyly of the big toe and ankle valgus deformity nor scoliosis and residual proximal femoral deformity of SCFE interferes with their daily living activities. One of them (IV-3) had even played basketball in a high school varsity team. However, development of unstable SCFE threatened function of the hip joint, and the proband was required to have major hip surgeries. SCFE is a chronic, gradual displacement of the femoral head at the proximal femoral physis. It may remain silent until physeal closure, and end up with residual deformity at the proximal femur as in the Patients III-3 and IV-

1 (Fig. 4). However, in some cases, the SCFE could aggravate suddenly, resulting in unstable separation of the femoral head as in Patients IV-2 and IV-4 (Figs. 3 and 4), which is an orthopedic emergency requiring surgical intervention to stabilize the femoral head and to preserve its viability. Hence, once this disease entity is recognized, the patient should have an orthopedic consultation to monitor development and progress of SCFE, which was exclusively harbored by the affected members in this family. It is noteworthy that a residual deformity of silent SCFE showed posterolateral displacement of the femoral head (Fig. 4), a rare subtype of SCFE [Loder et al., 2006]. Scoliosis did not require any intervention in these affected family members. Macrodactyly of the big toes were not complained of in shoe fitting or cosmesis in the proband and affected family members.

The characteristic clinical and radiological findings make it a specific, discernible clinical disease entity, which can be differentiated from Marfan or other related syndromes. However, it is very similar to a phenotype caused by chromosomal translocation of 2q37 and subsequent CNP overproduction [Bocciardi et al., 2007; Moncla et al., 2007]. Hence, CNP overproduction and its receptor gene gain-of-function mutation may be categorized into a disease entity, that is, overgrowth CNP/*NPR2* signalopathy, which should be included in differential diagnosis of the overgrowth syndrome.

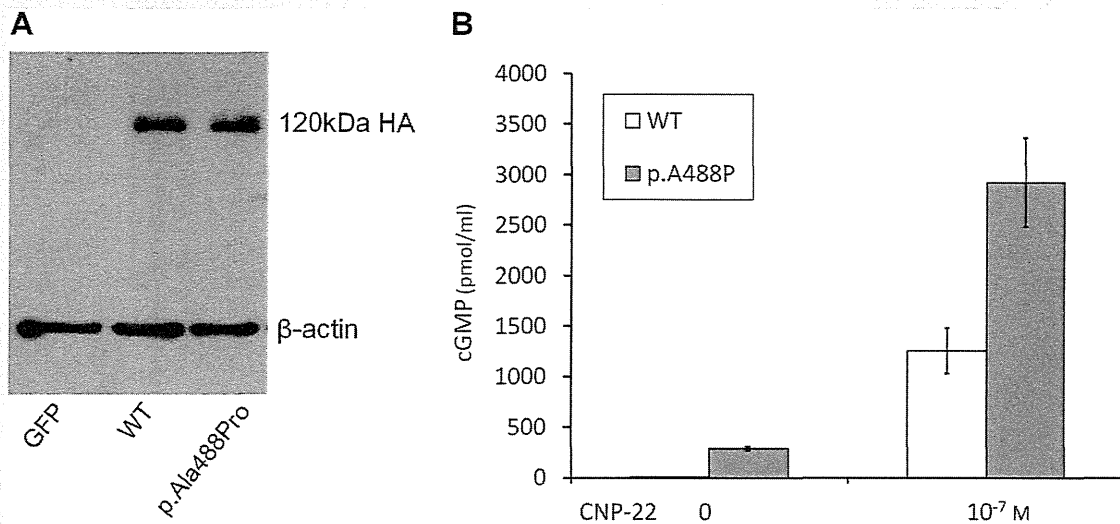


FIG. 6. NPR2 mutation of p.Ala488Pro is a gain-of-function mutation. **A:** Western blot analysis confirmed the comparable expression of HA-WT [WT] and HA-Ala488Pro. As an internal control, β -actin in each sample was detected with anti- β -actin antibody. **B:** Increased cGMP production in the HEK293A cells transfected with the p.Ala488Pro mutant compared to that in wild-type cells [WT]. Forty-eight hours after the transfection, the cells were serum-starved for 24 hr, and then treated with the indicated concentrations of CNP-22 for 10 min, before cGMP production was assayed. Results are presented as the mean \pm SD (N = 3, *P < 0.05).

In summary, we report on a family with an overgrowth syndrome inherited as autosomal dominant trait, which is caused by a gain-of-function mutation at *NPR2*. This is a distinct clinical entity that can be differentiated from other overgrowth syndromes by its clinical and radiological manifestations. Recognition of this specific disease entity will lead to targeted molecular study for confirmation, and will alert the clinician for potentially serious complication such as unstable SCFE.

ACKNOWLEDGMENTS

This study was supported in part by a grant from Ministry for Health, Welfare and Family Affairs, Republic of Korea (A080588) and in part by Grants-in-aid from the Ministry of Health, Labour and Welfare of Japan (KH20Q007a-1).

REFERENCES

- Bartels CF, Bukulmez H, Padayatti P, Rhee DK, van Ravenswaaij-Arts C, Pauli RM, Mundlos S, Chitayat D, Shih LY, Al-Gazali LI, Kant S, Cole T, Morton J, Cormier-Daire V, Faivre L, Lees M, Kirk J, Mortier GR, Leroy J, Zabel B, Kim CA, Crow Y, Braverman NE, van den Akker F, Warman ML. 2004. Mutations in the transmembrane natriuretic peptide receptor NPR-B impair skeletal growth and cause acromesomelic dysplasia, type Maroteaux. *Am J Hum Genet* 75:27–34.
- Bocciardi R, Giorda R, Buttgerit J, Gimelli S, Divizia MT, Beri S, Garofalo S, Tavella S, Lerone M, Zuffardi O, Bader M, Ravazzolo R, Gimelli G. 2007. Overexpression of the C-type natriuretic peptide (CNP) is associated with overgrowth and bone anomalies in an individual with balanced t(2;7) translocation. *Hum Mutat* 28:724–731.
- Chusho H, Tamura N, Ogawa Y, Yasoda A, Suda M, Miyazawa T, Nakamura K, Nakao K, Kurihara T, Komatsu Y, Itoh H, Tanaka K, Saito Y, Katsuki M. 2001. Dwarfism and early death in mice lacking C-type natriuretic peptide. *Proc Natl Acad Sci USA* 98:4016–4021.
- Hachiya R, Ohashi Y, Kamei Y, Suganami T, Mochizuki H, Mitsui N, Saitoh M, Sakuragi M, Nishimura G, Ohashi H, Hasegawa T, Ogawa Y. 2007. Intact kinase homology domain of natriuretic peptide receptor-B is essential for skeletal development. *J Clin Endocrinol Metab* 92:4009–4014.
- Take T, Kitamura H, Adachi Y, Yoshioka T, Watanabe T, Matsushita H, Fujii T, Kondo E, Tachibe T, Kawase Y, Jishage K, Yasoda A, Mukoyama M, Nakao K. 2009. Chronically elevated plasma C-type natriuretic peptide level stimulates skeletal growth in transgenic mice. *Am J Physiol Endocrinol Metab* 297:E1339–E1348.
- Loder RT, O'Donnell PW, Didelot WP, Kayes KJ. 2006. Valgus slipped capital femoral epiphysis. *J Pediatr Orthop* 26:594–600.
- Miura K, Namba N, Fujiwara M, Ohata Y, Ishida H, Kitaoka T, Kubota T, Hirai H, Higuchi C, Tsumaki N, Yoshikawa H, Sakai N, Michigami T, Ozono K. 2012. An overgrowth disorder associated with excessive production of cGMP due to a gain-of-function mutation of the natriuretic peptide receptor 2 gene. *PLoS ONE* 7:e42180.
- Moncla A, Missirian C, Cacciagli P, Balzamo E, Legeai-Mallet L, Jouve JL, Chabrol B, Le Merrer M, Plessis G, Villard L, Philip N. 2007. A cluster of translocation breakpoints in 2q37 is associated with overexpression of NPPC in patients with a similar overgrowth phenotype. *Hum Mutat* 28:1183–1188.
- Potter LR, Abbey-Hosch S, Dickey DM. 2006. Natriuretic peptides, their receptors, and cyclic guanosine monophosphate-dependent signaling functions. *Endocr Rev* 27:47–72.

- Schulz S. 2005. C-type natriuretic peptide and guanylyl cyclase B receptor. *Peptides* 26:1024–1034.
- Teixeira CC, Agoston H, Beier F. 2008. Nitric oxide, C-type natriuretic peptide and cGMP as regulators of endochondral ossification. *Dev Biol* 319:171–178.
- Tsuji T, Kunieda T. 2005. A loss-of-function mutation in natriuretic peptide receptor 2 (*Npr2*) gene is responsible for disproportionate dwarfism in *cn/cn* mouse. *J Biol Chem* 280:14288–14292.
- UniProtKB[Internet]. UniProt Consortium (EMBL-EBI, PIR, and SIB) [2002]. P20594(ANPRB_HUMAN) [updated January 9, 2013 Version 151, Cited January 12, 2013]. Available from <http://www.uniprot.org/uniprot/P20594>
- Yasoda A, Ogawa Y, Suda M, Tamura N, Mori K, Sakuma Y, Chusho H, Shiota K, Tanaka K, Nakao K. 1998. Natriuretic peptide regulation of endochondral ossification. Evidence for possible roles of the C-type natriuretic peptide/guanylyl cyclase-B pathway. *J Biol Chem* 273:11695–11700.

Review Article

Current Understanding on the Molecular Basis of Chondrogenesis

Toshimi Michigami¹

¹ *Department of Bone and Mineral Research, Osaka Medical Center and Research Institute for Maternal and Child Health, Osaka, Japan*

Abstract. Endochondral bone formation involves multiple steps, consisting of the condensation of undifferentiated mesenchymal cells, proliferation and hypertrophic differentiation of chondrocytes, and then mineralization. To date, various factors including transcription factors, soluble mediators, extracellular matrices (ECMs), and cell-cell and cell-matrix interactions have been identified to regulate this sequential, complex process. Moreover, recent studies have revealed that epigenetic and microRNA-mediated mechanisms also play roles in chondrogenesis. Defects in the regulators for the development of growth plate cartilage often cause skeletal dysplasias and growth failure. In this review article, I will describe the current understanding concerning the regulatory mechanisms underlying chondrogenesis.

Key words: chondrocyte, transcription factors, growth factors, extracellular matrix, differentiation

Introduction

In mammals, most of the skeleton including the long bones of the limbs and the vertebral columns is formed through endochondral bone formation, which consists of the mesenchymal condensation of undifferentiated cells, proliferation of chondrocytes and differentiation into hypertrophic chondrocytes, followed by mineralization (1–3). Proliferating chondrocytes form orderly parallel columns in the growth

plates, and are characterized by the expression of type II, IX, and XI collagen (Col II, IX and XI) and proteoglycans such as aggrecan. When chondrocytes differentiate, they become hypertrophic and begin to produce a high level of alkaline phosphatase and type X collagen (Col X). Eventually, the terminally differentiated chondrocytes undergo apoptosis, and the cartilaginous matrix is mineralized and replaced by bone (1–3). These mature chondrocytes express vascular endothelial growth factor (VEGF) and matrix metalloproteinases (MMPs) (4, 5). VEGF induces blood vessel invasion, and MMPs aid in the degradation of the cartilaginous matrix (4, 5). Accumulating evidence provided by human diseases, mouse models and cell studies has identified a number of factors to be involved in the regulation of proliferation and differentiation of chondrocytes (Fig. 1). Among them are various transcription factors, soluble growth factors, ECMs, and epigenetic factors. In this review

Received: August 13, 2013

Accepted: September 13, 2013

Corresponding author: Dr. Toshimi Michigami, Department of Bone and Mineral Research Osaka Medical Center and Research Institute for Maternal and Child Health, 840 Murodo-cho, Izumi, Osaka 594-1101, Japan
E-mail: michigami@mch.pref.osaka.jp

This is an open-access article distributed under the terms of the Creative Commons Attribution Non-Commercial No Derivatives (by-nc-nd) License <<http://creativecommons.org/licenses/by-nc-nd/3.0/>>.

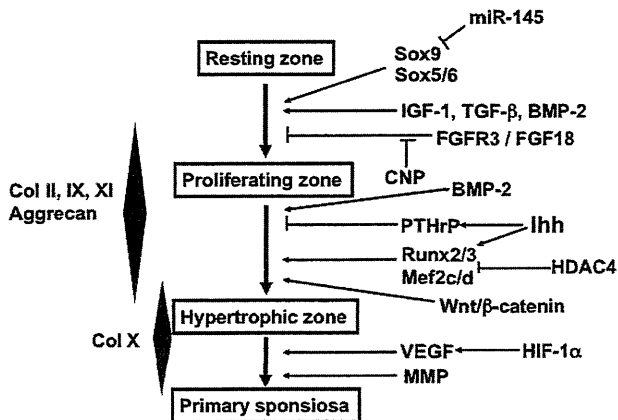


Fig. 1. Molecular network controlling the development of growth plate cartilage.

article, I will provide an updated overview of the molecular mechanisms regulating the development of growth plate cartilage.

Transcription Factors Involved in Chondrogenesis

Among the transcription factors involved in chondrogenesis, SOX9 has been the most extensively studied. SOX9 is a member of the Sox family of transcription factors characterized by a high-mobility-group-box DNA binding motif related to that of the sex-determining factor SRY, and is a responsible molecule for campomelic dysplasia characterized by severe skeletal malformation (6, 7). Evidence provided by mouse models has also revealed that Sox9 is indispensable for chondrogenesis. Sox9 begins to be expressed at the mesenchymal osteochondroprogenitor stage, and transactivates several genes specific to proliferating chondrocytes such as *Col2a1* encoding Col II (8, 9). Sox5 (L-Sox5) and Sox6 were shown to cooperate with Sox9 to activate the chondrocyte-specific enhancers in these genes (10, 11). The activating transcription factor (ATF)/cyclic AMP response element binding protein (CREB) family and the AP1 family member c-Fos are required to maintain the proliferative capacity of early chondrocytes (12, 13).

Hypertrophic maturation of chondrocytes requires the Runt domain family transcription factors Runx2 and Runx3 as well as a decrease in the expression and/or activity of the Sox proteins. *Runx2/Runx3*-double knockout mice lack hypertrophic chondrocytes (14, 15). It has been reported that Runx2 directly transactivates the genes *Ihh* (*Indian hedgehog*), *Col10a1* encoding Col X, and *MMP13* (15–17). Recently, it has also been shown that Sox9 suppresses the expression of Runx2 and β -catenin signaling, which inhibits the hypertrophic change of chondrocytes (18). A basic helix-loop-helix type transcription factor, Twist-1 functions as another repressor of Runx2 in the perichondrium (19). Other transcription factors, such as MADS-box transcription factors Mef2c and Mef2d (myocyte enhancer factor 2c and 2d), Msx2, the AP1 family member Fra2, and FoxA family transcription factors, also facilitate chondrocyte hypertrophy (20–25). The transcription factor hypoxia-inducible factor-1 α (HIF-1 α) is one of the major regulators of the hypoxic response in mammals and plays a role in chondrocyte survival and gene regulation for VEGF, which induces blood vessel invasion into cartilage (26, 27). Thus, a complex transcriptional network governs the process of chondrogenesis from chondrocytic commitment to terminal differentiation.

Soluble Regulators of Chondrogenesis

Fibroblast growth factors (FGFs) play critical roles in chondrogenesis by activating signaling through FGF receptors (FGFRs), as indicated by a spectrum of human chondrodysplasias and dwarfism caused by gain-of-function mutations in the *FGFR3* gene (28–31). Among the FGFRs, *Fgfr3* is expressed in cells undergoing mesenchymal condensation and proliferating chondrocytes. On the other hand, *Fgfr1* is expressed in prehypertrophic and hypertrophic chondrocytes (32–34). It has been suggested that FGFR3-mediated signaling negatively regulates chondrocyte proliferation and differentiation (35–

37). In FGFR3-related chondrodysplasias such as achondroplasia, constitutive activation of FGFR3 results in the activation of the downstream ERK and STAT pathways (28). Although various FGFs are expressed in cartilage, FGF18 is suggested to be a physiological ligand for FGFR3 in chondrocytes, because of similar histology in the growth plates between *Fgf18*-knockout mice and *Fgfr3*-knockout mice (38, 39).

Ihh is a secreted signaling molecule, expressed by prehypertrophic chondrocytes. A line of evidence provided by genetically altered mouse models has revealed that Ihh increases the expression of parathyroid hormone-related protein (PTHrP) in perichondrial cells and chondrocytes at the ends of long bones, which delays chondrocyte hypertrophy through the PTH/PTHrP receptor expressed in proliferating chondrocytes. Thus, Ihh and PTHrP function in a local negative feedback loop to regulate the onset of hypertrophic differentiation (40). In addition, it is also reported that Ihh stimulates the proliferation and maturation of chondrocytes independently of PTHrP, in which activation of Wnt and bone morphogenetic protein (BMP) signaling is suggested to be involved (41–43).

The importance of C-type natriuretic peptide (CNP) signaling in chondrogenesis was shown by the severe dwarfism of *CNP*-knockout mice (44, 45). CNP exerts its signal mainly through the receptor NPR2, which is also called guanylyl cyclase B (GC-B), and *Npr2*-null mice display a similar phenotype to *CNP*-knockout mice (46). Based on the mouse studies, it has been suggested that CNP promotes endochondral bone growth through several mechanisms, including the stimulation of chondrocyte proliferation and hypertrophy and an increase in ECM production (44–46). In humans, loss-of-function mutations in the *NPR2* gene cause acromesomelic dysplasia, type Maroteaux, characterized by severe dwarfism (47, 48), while a gain-of-function type mutation in the gene has been identified in a family with skeletal overgrowth (49), which indicates that the CNP/NPR2 signaling pathway

plays a role in the development of growth plate cartilage both in humans and mice. The similarity in the skeletal phenotype between CNP-deficient mice and human achondroplasia has suggested that CNP/NPR2 signaling is promising as a new therapeutic target for the dwarfism associated with skeletal dysplasia (46). It has been shown that the signaling evoked by CNP inhibits the FGF-induced activation of the ERK pathway (46). The p38MAPK pathway and PI3K/Akt pathway are also suggested to be involved in the regulation of chondrocyte development by CNP (50).

Other soluble factors such as Wnts, bone morphogenic proteins (BMPs), transforming growth factor-beta (TGF- β), insulin-like growth factors (IGFs) and thyroid hormone are also involved in chondrogenesis (51–53) but are not further discussed here.

Regulation of Chondrogenesis by the ECM

The ECM provides a cell type-specific microenvironment. As chondrocytes mature, they produce abundant ECM proteins such as collagens and proteoglycans, and the cell-matrix interactions come to have more important roles than in the earlier stages of chondrogenesis, when the cell-cell interaction via adhesion molecules such as N-cadherin and N-CAM is involved in cellular condensation and subsequent chondrogenesis (54, 55). The ECM is recognized and bound by integrins and cell surface transmembrane receptors. Integrins occur as dimers of an α subunit and a β subunit, and the binding of ligands to integrins leads to transduction of signaling from the ECM to intracellular effectors (56). Chondrocytes express several integrin subunits, and it has been reported that chondrocyte-specific $\beta 1$ integrin-knockout mice exhibited a chondrodysplasia-like phenotype (57, 58). In these mice, growth plates exhibited unorganized proliferative columns and an abnormal cell shape due to the loss of adhesion to Col II, and the isolated chondrocytes displayed

reduced proliferation (58). Integrin-linked kinase is one of the components of the complex whose formation is triggered by the activation of integrin-mediated signaling, and knockout of its gene resulted in a chondrodysplasia-like phenotype similar to that of chondrocyte-specific $\beta 1$ integrin-knockout mice (59). These results suggest the importance of integrin-mediated signaling from the ECM in chondrogenesis.

The *SLC26A2* gene encodes a sulfate transporter responsible for sulfate uptake by chondrocytes. Mutations in this gene have been identified in a form of chondrodysplasia called diastrophic dysplasia, which is characterized by undersulfation of cartilaginous proteoglycans. Similar to patients with diastrophic dysplasia, *dt* mice harboring a knock-in *Slc26a2* mutation were reported to exhibit undersulfation of glycosaminoglycans such as chondroitin (60). It has been also reported that mice lacking the gene encoding chondroitin sulfate *N*-acetylgalactosaminyltransferase 1 (CSGalNAcT-1), an enzyme involved in the initiation of the biosynthesis of chondroitin sulfate, have shorter, disorganized chondrocyte columns in the growth plates with a rapid catabolism of aggrecan (61).

Another function of the cartilaginous ECM is regulation of chondrogenesis through binding, storage, and release of soluble factors. For example, most of FGFs bind to heparan sulfate proteoglycans and bind to FGFRs in the context of heparan sulfate proteoglycans to trigger signal transduction. Analysis of mice lacking sulfate-modifying factor 1 (*Sumf1*) has suggested that desulfation of proteoglycans regulates chondrocyte proliferation and differentiation by limiting FGF signaling (62).

Vinculin is a major component of the focal adhesion complex and functions in adhesion and/or signaling between the extracellular microenvironment and the cell via integrins and cadherins. Although little is known about its tissue-specific functions, we have recently identified vinculin as having profound roles in

chondrogenesis (63). Knockdown of vinculin in primary chondrocytes and organ cultures of metatarsal explants resulted in reduced expression of *Col2a1*, *aggrecan*, *Col10a1*, and *Runx2*. Moreover, knockdown of *vinculin* abrogated IGF-I-induced growth of metatarsal explants. The upregulation of *Col2a1* and *aggrecan* expression by IGF-I was also cancelled by the knockdown. These results suggest that vinculin regulates the expression of chondrocyte-specific genes by orchestrating the signaling from the ECM and soluble factors such as IGF-I (63).

Epigenetic Control of Chondrogenesis

Recent studies have uncovered the roles of epigenetic mechanism in chondrogenesis. Among the histone deacetylases (HDACs), HDAC4 has been shown to prevent the premature chondrocyte hypertrophy by inhibiting the activity of *Runx2/3* and *Mef2c/d* transcription factors (20, 21, 64). HDAC1 and HDAC2 mediate the repression of some cartilage-specific genes including *Col2a1* (65). These findings suggest that histone modification influences the process of endochondral bone formation.

DNA methylation is also involved in the regulation of cartilage-specific genes. For example, it was reported that the demethylation of 2 CpG sites in the *COL10A1* promoter was correlated with induction of the *COL10A1* gene during the chondrogenic differentiation of human mesenchymal stem cells (66).

MicroRNAs as Novel Regulators of Chondrogenesis

MicroRNAs (miRNAs) are a class of ~22 nucleotide noncoding RNAs that regulate the expression of other genes at the posttranscriptional level. The critical roles of miRNAs in chondrogenesis were first indicated by the severe skeletal growth defects in mice lacking *Dicer*, an enzyme required for miRNA synthesis (67). In the growth plates of *Dicer*-